Elevated aeolian sediment transport on the Colorado Plateau, USA: The role of grazing, vehicle disturbance, and increasing aridity

Article *in* Earth Surface Processes and Landforms · June 2018

DOI: 10.1002/esp.4457

CITATIONS
32

READS
359

4 authors, including:

Travis Nauman
United States Geological Survey
35 PUBLICATIONS **952** CITATIONS

SEE PROFILE

Nicholas P. Webb
United States Department of Agriculture
97 PUBLICATIONS **1,930** CITATIONS

SEE PROFILE

Elevated aeolian sediment transport on the Colorado Plateau, USA: the role of grazing, vehicle disturbance, and increasing aridity

Travis W. Nauman[1], Michael C Duniway[1], Nicholas P. Webb[2], Jayne Belnap[1]

1 U.S. Geological Survey, Southwest Biological Science Center, 2290 SW Resource Blvd, Moab, UT 84532

2 USDA-ARS Jornada Experimental Range, P.O. Box 30003, MSC 3JER, NMSU, Las Cruces, NM 88003

Corresponding Author: T.W. Nauman, tnauman@usgs.gov, 001-520-664-5597

This article has been accepted for publication and undergone full peer review but has not been through the copyediting, typesetting, pagination and proofreading process which may lead to differences between this version and the Version of Record. Please cite this article as doi: 10.1002/esp.4457

Elevated aeolian sediment transport on the Colorado Plateau, USA: the role of grazing, vehicle disturbance, and increasing aridity

Abstract

Dryland wind transport of sediment can accelerate wind erosion, degrade air quality, mobilize sand dunes, and drive ecological change. These processes are associated with human health concerns, loss of water supply, decreased land productivity, infrastructure damage, and related economic impacts. We measured aeolian sediment horizontal mass flux (*q*) at 100 cm height using passive aspirated sediment traps on the Colorado Plateau in Utah, USA to better understand how wind transport of sediment varies with land use, climate, and environmental heterogeneity. Measured 'hot spots' of *q* rival the highest ever recorded including 7,460 g m^{-2} day^{-1} (spring 2009) in an off-highway vehicle (OHV) area near Hanksville, UT, but were more commonly 50-2,000 g m^{-2} day^{-1} in areas with heavy livestock or OHV use. The overall mean measured *q* on rangeland sites was 5.14 g m^{-2} day^{-1}, considerably lower than areas with moderate livestock use (9 g m^{-2} day^{-1}), heavy livestock use (19 g m^{-2} day^{-1}), and OHV use (414 g m^{-2} day^{-1}). In contrast, a similar area monitored with minimal soil disturbance averaged 1.60 g m^{-2} day^{-1} from 2007-2015. Annual *q* on all rangeland land use types (minimal use, livestock, and OHVs) generally increased with increasing annual temperature, increased winds, and decreasing precipitation. Measurements of *q* downwind of unpaved road sites averaged 13.14 g m^{-2} day^{-1} with a maximum observed seasonal *q* of 128.0 g m^{-2} day^{-1} along an actively producing oil well access road. Four of the five largest road *q* values (n=33 total) measured were adjacent to roads primarily used to access oil or gas wells. Spatial modeling suggests that ~92-93% of regional *q* occurs in rangelands versus ~7-8% on unpaved

roads. Our overall findings indicate that predicted future regional mega-droughts will increase aeolian sediment transport, which would likely add to wind erosion and dust emissions already elevated due to land use. Increased aeolian activity will potentially further compromise air quality, hydrologic cycles, and other ecosystem services.

Keywords

particulates, land use, aeolian transport mapping, off-highway vehicles, accelerated erosion, drought, fugitive dust, wind erosion

Introduction

Aeolian sediment transport, including sandstorms, wind erosion and blowing dust, is a major resource concern threatening the livelihoods and health of many around the globe (ELD Initiative, 2015; Okin et al. 2011; UNEP, WMO, & UNCCD, 2016). Concerns with aeolian sediment transport reflect impacts of increasing anthropogenic pressure on land globally, coupled with an increasing frequency and intensity of drought, particularly in drylands. A pivotal example of this phenomenon was the American Dust Bowl of the 1930s, where misguided land use policy and climate variation triggered extreme wind erosion and land degradation (Peters et al., 2007). During the Dust Bowl, plowing in semi-arid regions coincident with drought caused extreme wind erosion and general economic devastation (Cook et al., 2009; Hansen et al, 2004; Lee and Gill, 2015). There was a relatively rapid and effective institutional response to the Dust Bowl by the US Government, including the creation of the Soil Conservation Service and other US Department of Agriculture entities that spurred significant investments in soil conservation. Intensifying droughts (Schlaepher et al., 2017; Trenberth et al., 2014), fire impacts (e.g., Miller et al., 2014; Sankey et al., 2012), and increasing conflicts related to drought impacts on humans

in drylands globally (e.g., Gleick et al., 2014) have the potential to result in similar challenges to those experienced during the Dust Bowl. The challenge of maintaining healthy soils and mitigating erosion is one that has influenced the rise and fall of civilizations throughout human history, and continues to be a salient issue today for land managers and policy makers, particularly in drylands (ELD Initiative, 2015; Montgomery, 2007).

The Colorado Plateau in the southwestern United States has been identified as having a high risk of future drought (Ault et al., 2016; Cook et al., 2015) and increased wind erosion (Munson et al., 2011). The region also has co-occurring and potentially conflicting land-use types which vary at fine scales over a large area (Copeland et al., 2017), each with the potential to generate large quantities of dust due to vegetation and soil surface disturbance (Belnap and Gillette, 1997, 1998). Regional land uses of concern include energy and mineral extraction (Nauman et al., 2017; USDOI-BLM-CCDO, 2013), unpaved roads and trails (EPA-DRI-CSOSE, 2014; Gillies et al., 2005; Duniway and Herrick, 2011; Padgett et al., 2008), and livestock grazing (Belnap et al., 2009; Duniway et al. In Press; Flagg et al., 2014; Neff et al., 2008). Although fire has not been a significant influence on aeolian dynamics of Colorado Plateau drylands to date, it has in other similar drylands of the western USA (e.g., Miller et al., 2012). Dust can impact human health, primarily through respiratory ailments and traffic fatalities (Cook et al., 2005; Derbyshire, 2007; Griffin et al., 2001). Many of the regional shale formations on the Colorado Plateau (e.g., Mancos, Chinle, and Morrison Formations) have a variety of metals and other potentially hazardous inorganic constituents that could intensify these issues via exposure to dust emissions from soils derived from these formations (Morrison et al., 2012; Pliler and Adams, 1962; Statwick and Sher, 2017; Stokes and

Mobley, 1954). Dust deposition on the regional snowpack has raised concerns about resulting decreases in regional water supply (Painter et al., 2010; Painter et al., 2018). Large aeolian sediment horizontal mass fluxes during drought in the region have also been connected with sand dune mobilization and associated invasive plant encroachment which can both impair ecological function and damage regional infrastructure (Draut et al., 2013; Thomas and Redsteer, 2016). Regional outdoor tourism also relies on visual resources as an economic driver with some of the busiest national parks in the USA impacted by Colorado Plateau dust emissions (e.g., 1.58 million visitors to Arches NP in 2016, https://www.nps.gov/arch/learn/management/statistics.htm). The broad impacts of increased aeolian transport in the region highlight the importance of disentangling how dominant land uses interact with climate to influence aeolian processes regionally.

Spatial modeling of aeolian transport can help to understand which landscape processes are driving observed increases in regional dust emissions in the western US (Hand et al. 2017). Processes controlling wind erosion and dust emission operate at scales ranging from microns to global, making them difficult to accurately model mechanistically (using empirical or process-based erosion models; e.g., Wagner, 2013; Okin et al., 2006). Vegetation height, orientation and size of vegetation canopy gaps, soil type, soil cover, surface roughness, wind speed, and antecedent moisture may influence aeolian processes. Efforts to model and identify dust sources with remote sensing have utilized MODIS and AVHRR imagery (Baddock et al., 2009; Bullard et al., 2008; Chappell and Webb, 2016; Lee et al., 2012; Li et al., 2013; Lu and Shao, 2001; Parajuli et al. 2014). The Landsat archive was recently used at finer resolution to identify dust plume sources on specific

landforms where areas of heavy saltation flux impacts finer grained river terrace deposits in South Africa (van Holdt et al., 2017). Several studies have also used geostatistical methods to map spatial variability of sediment horizontal mass flux (*q*) (Chappell et al., 2003; Sterk and Stein, 1997). These studies demonstrate potential to use spatial data and Landsat-scale (i.e., 30 m spatial resolution) remote sensing to help understand aeolian processes in areas of differing environmental context and land use.

Uncertainty in mechanistic dust model applications often stems from a lack of standardized and high-quality field data to validate and determine model uncertainties (Shao et al., 2011; Webb et al., 2016; Webb et al., 2017). An underlying challenge is the difficulty of directly measuring dust emission (i.e., vertical flux) without expensive instrumentation. However, spatially-distributed measurements of *q* are more widely available using horizontally oriented, naturally aspirated sediment samplers (Fryrear, 1986; Fryrear et al., 1991). Although these aspirated sediment samplers do trap dust-sized suspended particles <50 um (Floyd and Gill, 2011; Chappell et al., 2003), they are generally inefficient (35-45% capture rate) and capture more of the saltation flux (Goossens and Buck, 2012; Goossens and Offer, 2000; Shao et al., 1993). Increased *q* can reflect and be a driver of changing rangeland condition and disturbance (Okin et al, 2001a,b; Thomas and Redsteer, 2016), wind erosion activity (Okin et al., 2006; Miller et al., 2012), sand dune mobilization (Draut et al., 2013), and increased dust emission if fine particles are available for release (Gillette, 1977; Lu and Shao, 1999; Shao, 2001). In practice, naturally aspirated sediment samplers capture some combination of suspended finer dust and sand-sized saltating particles depending on sampling

height, location roughness, vegetation present, wind speeds during sampling, and sediment sources.

This study uses a network of Big Spring Number Eight (BSNE; Fryrear, 1986; Fryrear et al., 1991) naturally aspirated sediment samplers to help disentangle the influence of various land uses and climate on *q* on the drylands of the Colorado Plateau near Moab, Utah. Moab is a popular destination for tourism, non-motorized outdoor recreation, and off-road vehicle enthusiasts, which also has energy and mineral extraction industries and wide-spread grazing of domestic livestock (Copeland et al. 2017). These diverse, and often conflicting land uses in the area make it an interesting region to study how these uses impact aeolian processes. Spatial modeling of *q* was used to compare the relative impacts of distributed rangeland land uses (livestock, OHV, and low land-use areas) and unpaved road networks (following similar workflow to Hengl et al., 2017; Nauman & Duniway, 2016) on aeolian sediment transport rates. Livestock activity, OHV use, and climate trends were examined by comparing *q* at groups of sites with differing intensities of these use types, but in similar soils and vegetation communities. Our specific study objectives included 1) examining the interaction of land-use, climate trends, and measured *q* over time; 2) spatial predictions of *q* on rangelands and unpaved roads as a tool to identify areas with increased aeolian activity that may be at risk of dune mobilization, wind erosion, and dust emission; and 3) using the *q* spatial predictions to estimate the relative importance of unpaved roads and rangelands for regional aeolian sediment transport.

Methods

Study Area

This study is focused on dryland portions of the Colorado Plateau near Moab, Utah, USA. The study area is a mainly a sedimentary lithological landscape that has been uplifted to 1200-2000 m above sea level and adjacent to a protruding laccolith mountain range (La Sals) rising above 3800 meters (Fig. 1). Major plant communities include saline shrublands dominated by mat saltbrush (*Atriplex corrugate*), greasewood (*Sarcobatus vermiculatus*) or shadscale (*Atriplex confertifolia*) and James' galleta (*Pleuraphis jamesii*). Saline shrublands also tend to have finer grained soils that are associated with regional shale formations. Non-saline shrublands are also extensive and dominated by blackbrush (*Coleogyne ramosissima*) at elevations ~1000-1700 m and big sagebrush (*Artemisia tridentata*) from ~1700-2000 meters. At elevations ~1500-2000 m with shallower soils, there are woodlands mostly dominated by pinon pine (*Pinus edulis*) and Utah juniper (*Juniperus osteosperma*). Areas with deep sandier soils tend to be more dominated by grasses including needle and thread (*Hesperostipa comate*), Indian rice grass (*Achnatherum hymenoides*), James' galleta, alkali sacaton (*Sporobolus airoides*), and blue gramma (*Bouteloua gracilis*). Grasslands also usually include a lesser shrub component (four-wing saltbush [*Atriplex canescens*], Blackbrush, sand sage [*Artemisia filifolia*], and ephedra [*Ephedra spp.*]) (Duniway et al., 2016).

Aeolian Horizontal Sediment Mass Flux Monitoring

To better understand the interactions among land-use, climate, and the effects of landscape heterogeneity on aeolian sediment transport, U.S. Geological Survey (USGS) scientists initiated a landscape-scale study monitoring sediment horizontal mass flux (q) on the Colorado Plateau in 2004 (Flagg et al., 2014). In response to recent increases in recreation and energy development in the region (Copeland et al. 2017), this monitoring network was expanded in 2010 to include unpaved roads used for a combination of recreation and extraction. Big Spring Number Eight aeolian sediment samplers (Fryrear, 1986; Fryrear et al., 1991) were used to monitor q at a variety of rangeland locations, unpaved road locations, and at an off-road or 'off-highway' vehicle (OHV) use area in southeastern Utah (Fig. 1). Mass of sediment collected from each BSNE (all at 100 cm height) was divided by the area of the BSNE opening (10 cm^2) and the time the collector was out (days) to derive q (g m^{-2} day^{-1}) (Flagg et al., 2014; Floyd and Gill, 2011). Rangeland and unpaved road reaches were monitored to help identify areas with potential q impacts on wind erosion activity, dune mobilization, rangeland condition, local infrastructure, and dust emissions. Saltating particles generally trapped in BSNEs can abrade the soil surface or fragment on impact, potentially releasing fine dust that can travel tens to thousands of kilometers from source (Lu and Shao, 1999; Okin et al., 2006). These fine dust particles degrade regional air quality and have been shown to reduce snow albedo in the Rocky Mountains, affecting snow melt and runoff (Painter et al., 2018). A subset of similar rangeland sites, unpaved road sites, and the OHV site have been monitored for a longer period, allowing for analysis of how q has varied with climate over time among different land uses. Samplers were generally collected seasonally in February-March, July-August, and in October-November

excepting some periods when resources were not available (i.e., rangeland sites for 11/2004, 3/2005, 11/2005, 7/2013, 3/2014, and 11/2014). In cases where sampling did not take place, sediment was collected at the next seasonal sampling period, so no time periods were actually missed. Samplers at OHV sites had additional collections during the spring dust season at bi-weekly to monthly intervals from March through July to capture samples before BSNEs were filled to capacity. Although BSNEs were deployed at 15 cm, 50 cm and 100 cm, this study only analyzes samples from 100 cm height at all sites to avoid sample size limitations at 15 and 50 cm where vegetation obstruction of BSNE rotation required significant data to be omitted despite vegetation trimming during every collection. We used linear regression to compare measurements at the 15 cm and 50 cm heights to the 100 cm collections to see if significant information is missed by omitting lower heights. We found that *q* measured at 100 cm represented most of the variation in the 15 cm and 50 cm measurements (Rangeland sites: 50 cm $R^2 = 0.91$, 15 cm $R^2=0.68$, 15+50 cm $R^2=0.80$; Road sites: 50cm $R^2 = 0.75$, 15cm $R^2=0.49$, 15+50 cm $R^2=0.58$). The strong models between the 100 cm samples with the 15 cm, 50cm and the sum of 15 cm plus 50 cm samples allow us to represent most of the relative variation in *q* at all heights just using the 100 cm sample. By using the 100 cm measurements there were fewer data gaps across time and space in the monitoring network, allowing for better spatial and temporal resolution in the data while losing minimal information about overall relative *q* values across the study region.

Rangeland monitoring sites: Aeolian sediment samplers (BSNEs) were set up at 66 sites across a variety of landscape settings and land uses (Flagg et al., 2014). The rangeland monitoring network was initially established in 2004 with a limited number of sites, and was expanded and adjusted over time to address varying local

concerns. Initially, BSNE samplers were installed in areas with two types of land use: 1) near (<100 m) to water tanks that are heavily used by cattle (with evidence of high erosion by wind and water, hereafter referred to as 'heavily grazed blowout'; n=6 sites),and 2) areas with evidence of moderate cattle activity ('moderately grazed'; n = 3 sites with regularly observed fresh dung, cattle footprints, and foraging signs). In 2007, additional BSNE samplers were added in areas with light to no cattle use ('light/not grazed') due to distance from water, fencing, and/or topography (n=8 sites ; Badger Wash Experimental Watersheds; See Duniway et al. In Press). Together, these three groups of sediment samplers in similar sites with regionally finer textured loam, silt loam, and silty clay loam soils (Mancos and Morrison shale derived soils; Flagg et al., 2014; Nauman and Duniway, 2016) provide an opportunity to understand how *q* varies among groups of similar sites qualitatively varying in cattle use. Sites added more recently were located to measure *q* across the other ecosystem types in the study area which tend to be much sandier and rockier (Flagg et al., 2014).

Unpaved road reaches: Thirty-three unpaved road reaches were chosen for BSNE monitoring (n=6 in 2010, expanded to 33 total in 2013). The original road sites (n = 6) were set up in 2010 in similar shale areas to the original rangeland monitoring locations. Sampling locations added in 2013 were selected to obtain a broader and more representative sample of unpaved road types regionally (based on use, native soil texture, and level of improvement). Road reaches were selected such that they were oriented perpendicular (NW to SE) to the regionally dominant southwesterly wind direction, similar in concept to the downwind sampling implemented by Field et al. (2012). Collectors were placed 2 m downwind of the road edge and were constrained in rotational domain to sample +/-15 degrees from the dominant

southwesterly wind direction. This sample design was selected to isolate road influence on *q*, while recognizing that this strategy only samples part of the total *q* associated with unpaved roads.

OHV monitoring sites: We sampled *q* at an OHV use area (n=2 sites) near Hanksville, Utah from 2009 to 2013, along with similar nearby areas with no permitted OHV use (referred to as 'OHV controls'; n=6 sites). These sites were used to compare with measurements at the rangeland and road sites during that same period. The OHV sites, grazing contrast sites, and the unpaved road sites established in 2010 are all located in similar shale soil and vegetation settings and span similar time periods, enabling *q* comparisons across land-use types.

Analysis of Land Use and Climate Trends in Sediment Mass Flux

Annual climate parameters were regressed against *q* at the shale sites within OHV and OHV controls, unpaved roads, and rangeland grazing sites (heavily grazed blowouts, moderately grazed, and light/not grazed sites). These sites all had periods of observation back to the mid-2000s that allowed us to test the association between sediment transport and climate parameters while also looking for potential differences in *q* among the differing intensities of grazing and vehicular use. Each of the groups had slightly different periods of observation, thus separate regressions were built to compare climate trends while best utilizing the full dataset to maximize statistical degrees of freedom. We omitted 2004 data from the climate trend analysis of heavily grazed blowout sites because of the reported reductions of stock from these areas that corresponded with a large decrease in dust from 2004 to 2005 (See Table 1, also Fig. 4 in Flagg et al., 2014). We used the 2005-2015 record at heavily grazed blowout sites for the climate regression to ensure consistent stocking rates. Although stocking rates were reduced from 2004 to 2005, these areas still

experience heavy cattle use (T.W. Nauman, 2017 - field observations). Climate data from the Canyonlands Airport weather station was used for all trend analyses (station = KCNY, accessed from http://mesowest.utah.edu/).

Bi-directional stepwise (using AIC) multiple regression (MASS package, stepAIC, direction = "both"; Ripley et al., 2013) was used to analyze temporal climate trends within land use groups of *q* monitoring sites. Cross validation of regression models was performed using a leave-one-out method due to small sample size (n=5-12). Correlation analyses were used to select variables with at least |0.3| correlation with *q* measurements and no co-correlations with other included covariates ($r > 0.7$). Variables used in these analyses included annual averages of *q* (target variable), temperature, precipitation, average sustained wind speed, average wind-gust speed, and percent of time with sustained wind >4.5 m s^{-1} (10 mph), >8.9 m s^{-1} (20 mph) , and >11.2 m s^{-1} (25 mph) at standard 10 m height. Variables selected from the correlation analysis were included in a bi-directional stepwise regression. With the climate variables selected from the stepwise regression, we tested for multiplicative or divisive interactions. When distributions of *q* values were skewed, natural logarithm or base-ten logarithm were used to normalize the data. The regressions were used to evaluate how climate could influence *q* across the land use groups.

Spatial Modeling and Analysis

Although *q* can vary greatly over space and time (e.g., Chappell et al., 2003; Sterk and Stein, 1997), we hypothesized that embedded spatial patterns of *q* could be modeled when integrated over multiple seasons by approximating local environmental factors related to aeolian sediment transport (e.g., Miller et al., 2012; Okin et al., 2006; Parajuli et al., 2014; Webb et al., 2014). Prior efforts have estimated wind erosion from spatial representations of vegetation cover and height,

soil particle size, and soil moisture, but had very limited validation data and coarse grids of ~50-100 km (Shao, 2008; Shao and Leslie, 1997; Lu and Shao, 2001). We aimed to use finer scaled 30 m resolution Landsat satellite imagery, digital elevation models, climate interpolations, a newly produced soil texture class map (Nauman and Duniway, 2016), and an ecological map (Lowry et al., 2007) to approximate vegetation dynamics, soil texture, soil moisture, and roughness to map *q* based on our field measurements. We employed an interpolative, empirical, environmental correlation workflow similar in concept to digital soil mapping (e.g., Hengl et al., 2017) to spatially predict *q* for every 30-meter pixel in our study area. These predictions were made from both the unpaved road and rangeland BSNE measurements based on *q* measured at 100 cm height and averaged at each location over our most spatially dense measurement period (spring of 2013 to the spring of 2015). These spatial predictions were made to facilitate comparison of the total *q* regionally on unpaved roads and rangelands (generally grazed, but not everywhere) to help understand the relative magnitude of *q* across major land use types and to identify areas more at risk for wind erosion and associated dust emission. Hourly vehicle traffic data were collected at unpaved road sites using TRAFx Gen III magnetic traffic counters with a detection range of 6 meters buried at 20 cm within 1-meter of the road surface (TRAFx Research, Canmore, Alberta). However, there is little information from the land management agencies (Bureau of Land Management and county road departments) by which to extrapolate our traffic data to the unmeasured and remote set of roads regionally (~12,500 km in our study area). The traffic data were also only weakly correlated with unpaved road *q* measurements ($r = 0.47$, $p = 0.005$, q [g m^{-2} day^{-1}] ~ traffic rate [vehicles/hr], $n=33$). We hypothesized that much of the variability unexplained by the traffic data would be

due to variation in the vehicle size and weight as well as natural aeolian processes occurring at those road sites that could be potentially captured by the empirical model. Many of the heavily used roads also have gravel surfaces not present on more remote roads, and this could be detectable by Landsat, possibly allowing for road use to be represented indirectly through its effects on road surface reflectance in the empirical spatial model.

Spatial models of *q* were made by regressing BSNE measurements (100 cm height) against an extensive database of environmental raster covariates with spatial coverage of the entire Colorado Plateau (Appendix A). Covariates were derived from the National Elevation Dataset (NED; Gesch, 2007; Gesch et al., 2002), Southwest ReGAP (SWREGAP; Lowry et al., 2007), PRISM climate dataset (PRISM Group, 2010), National Renewable Energy Lab wind potential layer and a USGS Landsat 8 top-of-atmosphere (L8TOA) composite from 2013 (for soil adjusted total vegetation index [SATVI] only, See Appendix B) and 2014 (for SATVI and spectral ratios) following Nauman and Duniway (2016). Landsat data were composited and downloaded using Google Earth Engine (Gorelick et al., 2017). A map of USDA soil particle size classes as modified by Nauman and Duniway (2016) was also included as a potential predictor variable. Processing included computing a suite of topographic and Landsat geologic indices to represent soil-lithologic-topographic variability at different scales (Appendix A). Developed areas, open water and agricultural lands were screened from the rangeland model rendering (SWREGAP classes N11, N21, N22, and N80; Lowry et al., 2007). All layers were co-registered to a 30-meter raster grid in USA equal area Albers projection using the NAD83 datum. The PRISM climate layers (including precipitation and temperature layers, see Appendix A) were resampled by cubic convolution to 30-meters to smooth

gradients and avoid larger pixel artifacts with interpretive recognition that the native 800 m PRISM spatial resolution only allows for coarse regional gradient representation.

The Utah road GIS database was used to spatially constrain the empirical interpolative spatial model of unpaved road *q* (UAGRC, 2015). The road spatial layer was rasterized using buffers created from selected dirt or gravel attributed road types (CARTOCODE) and surface type (SURFTYPE – poorly populated). The buffer length was computed based on five road width observations of each road type in ArcGIS high-resolution aerial imagery (Table 1). The buffer was created based on the median buffer radius observed by sampling of road type disturbance widths and dividing by two. Road segments were chosen by zooming into five contrasting parts of the study area and finding a road segment of each road type that appeared to be representative (e.g., not a cul-de-sac or abnormally wide stretch). A road buffer polygon layer was then created for all unpaved roads based on the road type buffer estimates and then rasterized to a 2.5 meter grid. Spatial modeling was based on covariate data at road center in line adjacent to the downwind BSNE.

Due to small sample sizes, bi-directional stepwise multiple regression based on information criterion (MASS package, stepAIC, direction = “both”, Ripley et al., 2013) was used to conduct the spatial predictive modeling in the R software platform (R Development Core Team, 2005). Cross-fold validation was used to verify accuracy and robustness of models using the DAAG R package (Maindonald et al., 2015). Factor variable levels were treated as separate binary dummy variables for initial stepwise model building. Only significant factor levels with replication were included as binary dummy variables in a final multiple regression used in predictions and for cross-fold validation. For spatial models, cross validation fold number was chosen to

produce fold sizes of ~6 to ensure consistent correlation of observed and cross validated values within each fold via the visualization tool in the DAAG package. Root mean square error (RMSE) and coefficient of determination (R^2) were reported for the cross-validated predictions of *q*. All variables were initially considered in the stepwise model. The smaller road dust dataset did not have enough degrees of freedom for this approach, so an initial correlation pre-screening was used to choose only variables with a correlation of greater than |0.15|. Both road and rangelands *q* distributions were highly skewed and required base-ten logarithm transformation before analysis. After models were built in R, they were rendered onto the original covariate raster grid using the 'raster' package in R (Hijmans et al., 2016). Predictions were back-transformed in GIS after raster rendering of the model in $\log_{10}$ scale.

To mitigate concerns of extrapolating our predictions into environments beyond our BSNE inference space (due to the ad-hoc nature of the BSNE monitoring locations), we masked all of our predictions to match the distribution of the covariates at the BSNE sites in three different data-driven scenarios. These involved limiting spatial predictions to pixels where environmental predictors were between 1) the maximum and minimum of all used quantitative raster covariates as a conservative approach, 2) the minimum minus 5% of that value through the maximum plus 5% of that value for all covariates used as a more liberal approach, and 3) the minimum minus 10% of that value for all covariates used through the maximum plus 10% of that value for all covariates as our most liberal approach. The inference space masking kept models from making predictions in areas dissimilar to where we monitored.

Calculating Unpaved Road and Rangeland Contributions to Regional Aeolian Horizontal Mass Flux

Aeolian *q* predictive regression maps were used to compare relative total aeolian sediment transport in rangelands to totals on unpaved roads. Both models were masked for proper sampling inference scenarios (discussed in preceding section) to keep models from extrapolating into areas not represented by the BSNE locations. To compare spatial models, predictions were initially back transformed from $\log_{10}(q)$ into *q* units (g m^{-2} day^{-1}). Predictions were made on a 30 meter grid (same as covariates), which assumes that the conditions in each 30 meter grid cell represent environmental conditions that relate to the *q* for that area. However, in order to resolve roads from rangelands, the 30 meter cells for each model were resampled to an identically placed 2.5 meter grid using the nearest neighbor approach in SAGA GIS (Conrad and Wichmann, 2011). Predictions of *q* were then summed for all road pixels and all rangeland pixels (at the 2.5 meter resolution) within the inference space limits to compare the relative regional magnitude of *q* occurring on unpaved roads and rangelands. Comparison was done by a simple ratio of the summed *q* from rangeland or road pixels to the sum of *q* at all pixels used in both models (e.g., % rangeland *q* = [summed *q* of rangeland pixels]/[summed *q* of rangeland pixels + summed *q* of road pixels] x 100). Pixels with larger *q* predictions than the maximum observed at field sites (less than 0.1% of pixels) were truncated to the observed maximum *q* value for relative rangeland/road regional *q* summations to prevent unrealistic extrapolations in regression trends from influencing the comparison.

Since the rangeland BSNEs sample from all directions, but the unpaved road BSNEs only sampled from +/-15 degrees perpendicular to road segments, we accounted for directional constraints on the sampling at unpaved roads in comparisons of summed spatial predictions. To do this, regional weather station anemometer data were analyzed to estimate road *q* from all directions based on the relative proportion of winds not captured by the directional sampling. To calculate this proportion, a wind speed threshold had to be chosen for calculations. Flagg et al., (2014) found that maximum sustained wind speed (not gust) at local climate stations over their seasonal sampling period had the strongest association with *q* of all the variables they examined ($r = 0.63\text{-}0.70$, $p < 0.001$). In that study, Flag et al., (2014) also found that 5.5 m s^{-1} and 6.3 m s^{-1} were important threshold maximum sustained wind speed values above which most high *q* measurements occurred. Based on the Flag et al., (2014) results, we calculated annual proportions of time with southwesterly winds (180-270 degrees) at five local weather stations (LSL, KCNY, HWYU1, PPCUT, GREU1 from http://mesowest.utah.edu/), including the station still available from the Flagg et al., (2014) study (KCNY). We did so for three different wind speed cutoffs easily interpretable by local land managers, yet still consistent with the previous results (>4.4 m s^{-1} [10 mph], > 6.7 m s^{-1} [15 mph], and > 8.9 m s^{-1} [20 mph]). The ratio of total time above these cutoffs to total time of southwesterly winds above the various cutoffs were computed (e.g. [Overall % time > 4.4 m s^{-1}]/[% time > >4.4 m s^{-1} out of southwest]). Then, the ratios over the three wind speed cutoffs, which ended up being very similar (shown in results), were averaged to calculate a regional wind upscaling ratio.

The calculated upscaling ratio was used to adjust unpaved road *q* predictions to better represent potential periods of time with wind that could have produced *q* not captured due to directional constraints of the BSNE samplers. We assumed that our observed southwesterly collected *q* measurements across all unpaved road sites were proportional to the amount of time local weather stations recorded above the identified wind speed thresholds recorded from southwesterly directions. From this, we assumed that our *q* measurements could be up-scaled to account for other wind directions after regional aggregation by correcting for the ratio of total time with potential *q* producing winds to total time with potential *q* producing southwesterly winds. For example, if on average, the weather stations showed that 50% of *q* potential winds came from southwesterly directions (180-270 degrees), then the *q* predictions would be doubled for unpaved roads. We acknowledge that this assumption is an over-simplification where road reaches vary in their site context due to limiting sampling locations to those running perpendicular to southwesterly dominant winds, but not accounting for the sampling limitation would also be an obvious underestimation of *q* on unpaved roads. It is likely that roads running parallel to the dominant wind direction might have higher q values than we estimated in the spatial models due to their longer fetch distance (Okin et al., 2006). We only upscaled *q* predictions for summation calculations of unpaved road *q* spatial predictions over the study area for comparison to summed rangeland spatial *q* predictions where we could assume that the overall local directional variability in winds was likely to average out regionally.

Results

Climate and Land Use Trends in Measured Horizontal Sediment Mass Flux

All rangeland and OHV dust monitoring sites exhibited strong positive trends of *q* with differing combinations of annual temperature, higher annual wind speeds, and/or decreasing precipitation (Table 2, Fig. 2). The OHV and heavily grazed blowout sites had larger and more variable *q* measurements than the other land uses (Fig. 2). The OHV control and light/not grazed sites had much lower *q* values and less variability overall than grazed and OHV sites. All regression models accounted for at least 60% of the measured *q* variability across sites. However, cross validation produced a low outlier prediction for 2009 in the moderately grazed sites, while the rest of the validation values were predicted moderately well (R^2 = 0.55, RMSE = 2.71). The OHV model was not as statistically robust as the other models (p = 0.18 and poor cross validation), but it did explain 92% of the measured variability and had a very small sample size (n=5). Measured *q* at the heavily grazed blowout sites was most correlated to precipitation (r= -0.68, p=0.02, $\log_{10}(q)$~precip.), but multiple regression identified an interaction where precipitation effects decrease as wind speeds increase and become the dominant associated variable to aeolian sediment transport during years with the highest wind speeds and precipitation. At moderately grazed sites, *q* correlated most with annual temperature (r = 0.60, p = 0.04), but temperature also interacted inversely with precipitation - decreasing the association of increased *q* with increasing temperatures during wetter years. At light/not grazed sites, *q* was also most correlated to temperature (r = 0.62, p = 0.08), but in the selected regression, an interaction term suggests that large wind speeds at lower temperatures also were associated with larger *q* values.

Average *q* values in rangeland sites showed a pattern varying by use intensity. Heavily grazed blowout areas averaged 19.2 g m^{-2} day^{-1} (SE = 4.08), moderately grazed sites averaged 8.77 g m^{-2} day^{-1} (SE = 2.84), and light/not grazed areas averaged 1.60 g m^{-2} day^{-1} (SE = 0.12). Larger *q* values were observed at all sites in 2012, a year with both high temperatures and low precipitation (Fig. 2). Measured *q* values as large as 966 g m^{-2} day^{-1} were recorded in heavily grazed blowout areas during the spring of 2009 (low precipitation year) with fluxes higher than 400 g m^{-2} day^{-1} observed as recently as the spring of 2012. Measured *q* values between 50-750 g m^{-2} day^{-1} were observed through the record at three of the heavily grazed blowout sites and three of the moderately grazed sites east of Green River, Utah.

Observations of *q* as large as 7,460 g m^{-2} day^{-1} (spring 2009, dry year; Fig. 2) were measured in the OHV area sampled near Hanksville, Utah, with a measurement of 560 g m^{-2} day^{-1} in the last year measured (2013). Fluxes larger than 2,000 g m^{-2} day^{-1} were consistently observed at one of the OHV sites during the springs of 2009, 2010, 2011, and 2012. OHV sites had much larger annual average *q* values (mean: 414 g m^{-2} day^{-1}; SE: 65.9) than nearby OHV control sites (mean: 6.73; SE: 3.35) and road reaches included in regression analysis (mean: 8.11; SE: 0.37). Flux at both OHV and the OHV control sites had strong positive associations with percent of time with wind >4.4 m/s and decreasing precipitation. Values of *q* at the OHV sites also had a negative association with temperature, differing from the relationships seen in the rangeland regressions. However, the negative correlation could reflect less OHV use during years with hotter than average temperatures. Base-ten normalized *q* values at the OHV control sites co-varied with a multiplicative interaction between precipitation and percent of time with wind >4.4 m s^{-1}, indicating that precipitation had a larger association with decreased *q* in years with longer

periods of wind >4.4 m s^{-1}. Inversely, percent of time >4.4 m s^{-1} had a greater positive association with increased *q* in drier years. Both the OHV and OHV control climate regressions represented large portions of the measured *q* variability (R^2>0.9).

Unpaved road *q* trends from 2010-2016 had no correlations with any climate variable or trend over time (Fig. 2). The largest *q* measured at road sites was 128.0 g m^{-2} day^{-1} in the spring of 2013 on an active oil well access road. Four of the five largest road *q* measurements were along roads that predominantly provide access to active oil or gas wells, while the fifth road services both recreational and oil and gas areas. There is a visible upward trend in *q* along unpaved roads from 2014-2016, but no statistically robust trend evidence (Fig. 2). Measured *q* from 2013-2015 appear to be relatively normal in both the road and rangeland monitoring networks (Fig. 2). This helps contextualize the spatial models built in the next section as representing somewhat normal years for aeolian sediment transport within our period of observation.

Spatial Models of Horizontal Sediment Mass Flux

Empirical spatial models of both the road and rangeland *q* had similar performances and were able to account for about 50-60% of the variation in the data and 30-40% in cross-fold validations (Tables 3 and 4). Cross-fold validation of the models showed root mean squared errors (RMSE) of about 1.5-2.0 g m^{-2} day^{-1} (back transformed from log10 scale). Both models included red spectral ratio indexes, SWREGAP classes, and aspect variables as predictors, but varied in other predictors selected for the models. Interestingly, the red spectral ratio indexes in both models were the most statistically significant and had very similar positive

coefficient estimates. These red ratios generally represent different native soils or road surfacing materials, but also could be picking up some vegetation greenness or senescent vegetation cover signal.

Modeled rangeland *q* values were generally largest in the northern portion of the study area in the Mancos shale salt desert, but were also large across Arches National Park (ARCH, north of Moab, Fig. 3) and areas along the east border of Canyonlands National Park (CANY, south-southwest of Moab, Fig. 3). The stepwise regression selected a large number of variables for this model which make it difficult to interpret each coefficient specifically (Table 3), but it is clear that spectral data, topography (relative height, slope, aspect, and landform), and ecotype/vegetation (SWREGAP) are significantly associated with spatial variability in *q*. The negative association of *q* with the 2014 SATVI likely reflects the stabilizing effect of vegetation on aeolian sediment transport. Annual precipitation and temperature also were selected, but were not significant coefficients at the 0.05 alpha level. The varying coefficients with spectral ratios, particularly with the different red ratios, indicate that very specific spectral signatures, likely associated with mainly geologic/soil variation, may be mediating *q*. Highly significant positive coefficients with elevation relative to the mean in an 8-pixel radius (relmnht8, Table 3) and slope gradient (slplp3, Table 3) seem to highlight some open and more exposed locations as associated with increased *q*. The significant negative relationship with relative elevation to minimum elevation in 1-pixel radius (relht1, Table 3) and the positive association with topographic wetness index (twilp3, Table 3) indicate that the lowest positions within ~45 meter radius scales and some drainages are associated with more *q*; possibly highlighting areas that act to concentrate wind energy through topographically connected low points. There was also a strong association between areas mapped

as ‘Invasive Southwest Riparian Woodlands and Shrubland’ communities by Lowry et al., (2007) and larger *q* predictions. These communities and topographic settings are often invaded by the non-native annual grass *Bromus tectorum,* and prone to dominance of bare ground and active erosion (Duniway et al. 2016).

Spatial variability in unpaved road *q* measurement*s* was very strongly associated with spectral patterns derived from Landsat with the normalized red to green spectral index (redgreennd, Table 4), accounting for 27% of the variance alone (p=0.002). It is likely that this was detecting soil, geologic, and/or varied road surfacing materials. It is also possible that adjacent vegetation added some signal to the redgreennd layer. For example, Fig. 4 shows an area where redder and finer soils from Kayenta sandstone are mixing with lighter colored Navajo sandstone soils of coarser texture, which seems to be influencing modeled *q* values. These spectral bands might also be picking up gravel, caliche, or magnesium sulfate applications on roads which would generally not have the redness component of common local sandstones. These road surfacing techniques might also be correlated with areas of higher use and thus be a surrogate for traffic. The road model also exhibited weaker associations of increased *q* with areas with lower ratios of summer to annual precipitation, south facing aspects, some vegetation types (SWREGAP), higher elevations, and certain native soil types (Table 4).

Regional Wind Direction Analysis

Five regionally co-located weather stations showed that the proportion of winds that originate from the southwest (180-270 degrees) were relatively consistent. Southwest winds accounted for an average of 40.8% (std. dev. = 0.013%) of all winds over 4.4 m s^{-1} (10 mph), 6.7 m s^{-1} (15 mph) and 8.9 m s^{-1} (20 mph). Southwesterly proportions were also consistent across weather stations for each

wind speed threshold (std. dev. from 5.8% to 8.6%). The relatively consistent proportionality of southwesterly winds across wind speed thresholds and weather stations provided further support for using an average of these ratios to regionally upscale unpaved road *q* estimates. An unpaved road *q* upscaling factor of 2.45 was calculated from the 40.8% average proportion of southwesterly winds by dividing into 100% (i.e., 100%/40.8%).

Regional Horizontal Sediment Mass Flux: Unpaved Roads versus Rangelands

Spatially summed *q* values for the study area show that rangelands account for about 12 times more *q* than unpaved roads in aggregate (roads 7-8% versus rangelands at 92-93%) (Table 5). After masking the rangeland maps for developed areas and both rangeland and road models for inference space constraints, it is clear that the larger area rangelands occupy is driving their overall larger summed regional flux. However, only 52-66% of all the study area rangelands were represented by the field measurements (based on inference space analysis), whereas 74%-89% of unpaved roads were represented by sampled road reaches. The smaller proportion of rangelands represented by the model indicates that the rangelands would potentially have an even larger contribution to regional *q* if a more complete sample had been taken (see Table 5: '% of Total Potential Model Area*'). The wind-corrected averaged predicted unpaved road *q* values (per area) across the spatial model was ~39 g m^{-2} day^{-1}, roughly seven times larger than the average predicted rangeland value of ~5.5 g m^{-2} day^{-1}. The much higher regional unpaved road *q* per-area average indicates that unpaved road expansion could increase regional *q* significantly.

Discussion

Accelerated Aeolian Sediment Transport: OHV use, Grazing, and Dust Emission Potential

We observed *q* values as large as almost any measured flux in the literature at 1-meter height with comparable sediment samplers (7,460 g m^{-2} day^{-1} near Hanksville, Utah in a Mancos shale off-road vehicle site in spring of 2009) (compare to Belnap et al., 2009; Miller et al., 2012). In studies that have recorded similar *q* quantities, these values correspond with extreme disturbance due to fire (Miller et al., 2012), or heavy grazing pressure (Belnap et al., 2009). Values of *q* >2000 g m^{-2} day^{-1} were observed during the springs of 2009, 2010, and 2011 at the OHV site, indicating a persistent potential for extreme levels of aeolian sediment transport. This is also true to a lesser degree east of Green River where Flagg et al. (2014) noted large sediment mass fluxes in heavily grazed areas. Although our analysis confirms the drop in average *q* values that Flagg et al. (2014) found when grazing pressure decreased in 2005, some of the heavily grazed blowout sites have continued to produce greater than 200 g m^{-2} day^{-1}, with a peak *q* of 966 g m^{-2} day^{-1} recorded at a site in the spring of 2009. These consistently large *q* values measured at some of the heavily grazed sites, even after some reduction in cattle numbers in 2005, suggests that soil stabilization in these areas has not yet been achieved, especially when compared to the light/not grazed locations (all *q* measurements <2.0 g m^{-2} day^{-1}). This is consistent with the concept of a persistent alternative ecological state in ecological state and transition theory. These degraded states (termed “annualized-bare” by Miller et al. [2011]) are characterized by decreased ecosystem function due to loss of protective biological soil crusts, increased bare ground exposure, large

decreases in perennial native vegetation, exotic plant invasions, high *q*, wind pedestalling, and, in more extreme cases, dune mobilization and gullying (Draut et al., 2012; Duniway et al., 2016; Miller et al., 2011; T.W. Nauman, 2017 - field observations; Fig. 5). Areas that have been pushed into such degraded ecological states are often unable to recover biotic and hydrological functioning autogenically, necessitating active management intervention (e.g. Bestelmeyer et al., 2009; Fick et al., 2016; Miller et al., 2011; Webb et al., 2014)(Fig. 5). Absent active intervention to restore these degraded areas, these ecosystems will likely remain with diminished capacity to support protective vegetation cover, be characterized by accelerated wind erosion, and be a source of dust emissions (Webb and Pierre, 2018).

However, at present these annualized-bare areas with large *q* values are relatively localized and generally fit the 'hot spot' concept posited by Gillette (1999). A phenomenon observed at some hot spots (e.g., site shown in Fig. 5) is upwind saltating sands blowing onto higher-clay soils of the Mancos and Morrison shales, thereby initiating dust emission from otherwise stable soils. Of further concern is the elevated concentrations of uranium, vanadium, selenium, and other associated metals and salts in Mancos and Morrison geologic formations which could be mobilized with dust emission events (Morrison et al., 2012; Pliler and Adams, 1962; Statwick and Sher, 2017) and have downwind consequences (e.g., Sankey et al., 2012). Indeed, part of the motivation for this study was a dust event from these areas in 2003 that caused car accidents on Interstate-70 downwind (Jayne Belnap, personal communication; Flagg et al., 2014). Interestingly, research has shown that soils in the Mancos shale can quickly form physical crusts (Godfrey et al., 2008) that may help protect against dust emission if sites are protected from surface disturbance and saltating sands from upwind areas.

Temporal, Climate, and Land Use Trends

Long-term patterns of *q* among land-use types show that aeolian sediment transport in all areas except roads tended to be closely related to climate (annual temperature, precipitation, and wind), but with combinations of parameters depending on land use. The magnitude of variability in *q* associated with climate variability was much larger in disturbed settings (OHV and heavily grazed blowout sites), likely due to the larger overall *q* values associated with more disturbance (Fig. 2). Although heavily grazed blowout sites showed relationships with climate variables, some areas still produced large *q* values (up to 560 g m^{-2} day^{-1}) during the relatively normal climatic period of 2013-2015 used for spatial predictions, providing further evidence that these sites may be in a persistent annualized-bare ecological state (see Bestelmeyer, 2006; Bestelmeyer et al., 2009; Miller et al., 2011) - especially when compared with the light/not grazed Mancos shale flux observations (mean *q*: 1.60 g m^{-2} day^{-1}; std. dev. = 0.33; SE = 0.12 for the entire 2007-2015 period).

All annual rangeland (grazing and OHV) *q* values were correlated with climate parameters. The trends were similar to those found by Reheis and Kihl (1995) that showed negative associations of annual dust deposition patterns with annual precipitation. These correlations also corroborate modeling work by Munson et al. (2011) that indicate higher temperatures and less available water will lead to increased wind erosion in this region. This trend of increased wind erosion is likely to increase further with projected higher temperatures and drought conditions by the end of the 21st century (Ault et al., 2016; Cook et al., 2015) due to reduced plant cover, even in areas with small amounts of disturbance. As more disturbed sites already have elevated aeolian sediment destabilization, changes in climate are likely

to produce synergistic increases in aeolian sediment transport proportional to the already elevated levels, potentially magnifying the effects of disturbance.

Spatial Variability and Landscape Controls

The spatial regression models' abilities to account for roughly half the variation in *q* averaged over two years suggests relatively strong covariation of aeolian sediment transport with bio-geophysical factors, similar to observations in other studies (Okin et al., 2006; Shao and Leslie, 1997; Webb et al., 2014). While our spatial models must be interpreted with caution (i.e., it is possible that evaluating individual pixels may not be appropriate), they do provide spatial depictions valuable for comparing regional *q* magnitudes and understanding their patterns at a landscape scale. The consistent use of Landsat spectral data in the red, blue and shortwave infrared wavelengths (redbluend, redgreennd, redswirnd, satvi14, swir1swir2nd) for predictions were probably detecting inherent erodibility differences of the contrasting soils and vegetation cover present (negative satvi14 coefficient in rangeland model) (Miller et al., 2012; Webb et al., 2014). Interestingly, red ratio indexes were the most significant variables in both models, suggesting that local sediment characteristics are important in *q* dynamics for both cases. For roads, this may also represent a contrast between surfaced (e.g., graveled) and unsurfaced (e.g., native soil) roads. Both models also include topographic and climate-related variables as predictors making more specific interpretations on regressions difficult, especially for the more complicated rangelands model. The negative relationship of SATVI with the rangeland sediment mass flux is intuitive, as larger SATVI values usually indicate more vegetation and less exposed soil (Marsett et al., 2006; Poitras et al., 2017; Villarreal et al., 2016).

Comparison of Aeolian sediment transport on Rangelands and Unpaved Roads

Analysis of predicted maps of *q* suggest that rangelands have a larger potential to initiate regional wind erosion and dust emissions than unpaved roads (92-93% versus 7-8% of q) due to the much greater areal extent of rangelands. However, predicted *q* values were 12 times greater on average (per-area) on unpaved road than rangeland sites. Particle size analysis of collected *q* samples would be necessary to determine how much of the collected sediment was dust sized (e.g., < 50 µm) and likely to be transported in suspension (e.g., Chappell et al., 2003; Floyd and Gill, 2011). The importance of aeolian sediment source extent versus per unit area flux rates has also been documented in other studies. For example, Reheis and Kihl (1995) found that although playas are more productive sources of dust per unit area than other sources, the greater area of non-playa sources were more important to overall regional dust deposition in southern California and Nevada.

The maximum measured seasonal unpaved road *q* was much lower than the maximum seasonally measured *q* at the heavily grazed blowout sites (Fig. 5; 128.0 g m^{-2} day^{-1} ,without wind correction versus 966 g m^{-2} day^{-1}), indicating that rangelands in an annualized-bare state can experience more aeolian sediment movement than active unpaved roads. We also noted that the unpaved road sites with the largest *q* values were generally associated with oil or gas well access, where heavier vehicles with larger tires were likely to have mobilized more sediment than passenger cars associated with regional tourism (Gillies et al., 2005). In rangelands, sites with more intense cattle use mobilized considerably more sediment than sites with more

moderate levels of cattle activity, consistent with other findings in similar ecosystems (Aubault et al., 2015; Belnap et al., 2009; Flagg et al., 2014). Additionally, the rangeland spatial models also captured areas of off-highway vehicle use (both in designated areas as well as unsanctioned off-road activity). The White Wash Sand Dunes OHV area was partially in the spatial model and was predicted to have larger sediment mass fluxes of around 100 g m^{-2} day^{-1}, but differs in substrate (sandy soils) from the shale lithology at the OHV *q* monitoring sites in this study. It is notable that these sand dunes mark the leading edge of a large series of sand dunes in the San Rafael Desert to the southwest that may reflect a trend towards desertification in the region and warrant further study. Other sandstone-dominated areas in the south part of Arches National Park and along the eastern border of Canyonlands National Park also had larger observed and modeled *q* values (Fig. 3). Areas within park boundaries with higher *q* values are not attributable to current domestic grazing as livestock have been excluded from Arches and Canyonlands since the 1960s. Rather, this could be due to the local soils originating from geologic formations with high proportions of silt, fine sands, and very fine sands that are prone to wind erosion when left unprotected from wind (United States Department of Agriculture, Natural Resources Conservation Service, 2010a, b). Even though grazing has been excluded from these parks for >50 years, vegetation and biological soil crusts in many areas impacted by historical cattle use have not recovered and as a result may still be erosion prone if not actively restored (Fick et al., 2016; Miller et al. 2011).

Implications for Land Management

Our results indicate that surface disturbance due to human land use can cause elevated aeolian sediment transport in our study area on the Colorado

Plateau, and that impact of disturbance on transport is compounded during hotter, drier and windier years. Increased trampling of dryland environments by livestock has been shown to increase sediment yields, often due to the loss of stabilizing biological soil crusts (Belnap and Gillette, 1997, 1998; Belnap et al., 2007; Belnap et al., 2009). Modelling work by Munson et al (2011) suggests that biological soil crusts, if left intact by lack of soil surface disturbance, can prevent sediment movement in these ecosystems even with a total loss of plant cover.

Our work indicates that aeolian sediment transport in the study area is potentially quite high relative to rates in other undisturbed rangeland ecosystems, and are likely to increase in the future with hotter and drier conditions. History provides examples of the risks posed by aeolian transport in dryland ecosystems by soil disturbing land-use activities during drought (e.g., Bestelmeyer et al. 2011; Miller et al. 2012; Peters et al. 2007; Yao et al. 2006) as well as new policy and associated management changes that have shown success in mitigating wind erosion (e.g., advent of the Soil Conservation Service and the National Grazing Service; Egan 2006, Sayre 2017). There is evidence that reductions in wind erosion in our study region were achieved following the Taylor Grazing Act (1934), but it also appears that wind erosion rates still have not returned to those estimated for pre-Anglo colonization (Neff et al. 2008). The observations and model results presented here suggest that large portions of the study region are still potentially affected by unsustainable wind erosion rates. However, our results also suggest that reducing surface disturbing activities by livestock and vehicles, especially during drought, may be effective strategies for reducing aeolian sediment transport and associated potential wind erosion and dust emissions. Areas in persistent annualized-bare ecological states may need more active restoration such as planting of vegetation,

biological soil crust remediation, and other erosion control measures (Fick et al., 2016; Field et al., 2009). Although regional management actions are unlikely to affect future climate trajectories that are likely under future drought scenarios (Ault et al., 2016), the results of this work suggest that new management strategies may be needed to prevent synergistic increases in aeolian sediment transport. Management strategies could focus on restoration of areas with current high horizontal mass flux as well as prevention of new high flux areas through a combination of (not ordered by significance) (1) management of off-road vehicle use; (2) limits on unpaved road network proliferation; and (3) livestock management focused on dust abatement, especially during hot, dry, and windy periods. This is particularly important for areas of the shale salt deserts (Mancos, Chinle, and Morrison formations) and sandy areas upwind of them that could be major sources of potentially toxic dust.

Conclusions

In this study, we provide evidence that the interaction of climate and land-use are contributing to elevated aeolian sediment transport on the Colorado Plateau, USA. These results suggest that land management actions could be implemented that partially abate dust impacts regionally. New data, maps, and synthesis show that unpaved road aeolian sediment horizontal mass fluxes (q) are several times greater per unit area than rangelands, but that rangelands likely account for more than 90% of regional q relative to roads due to the much greater area occupied by non-road drylands on the Colorado Plateau. Empirically derived q maps show promise to help guide management actions to assess and mitigate aeolian activity. Increased rangeland aeolian sediment transport was associated with surface disturbance due to livestock and off-road vehicle use on sensitive soils and landscape settings. The largest observed q in an off-road vehicle use area was

among the largest ever recorded. Elevated aeolian sediment transport rates can initiate dust emissions from finer grained regional shale-derived soils, posing potential human health risks. Dust emissions from the study area may also lead to surface water supply losses due to accelerated regional snowmelt, decreased human well-being by negatively impacting health, and negatively impacting local tourist economies by reducing visibility and view shed quality. We also observed that both disturbed and undisturbed rangelands have larger measured *q* values during years with higher temperatures, particularly when combined with more erosive winds and low precipitation. At present, much of the Colorado Plateau study region appears to be experiencing accelerated rates of wind erosion likely to be exacerbated by future climate change, increased surface disturbing land uses, or both.

Acknowledgements

Funding for this work was provided by the U.S. Geological Survey Priority Ecosystems Sciences Program, and Land Resources and Ecosystems Mission Areas, as well as the U.S. Bureau of Land Management. We would like to thank Bill Jackson and David Vaughan from the Grand County Roads Department for their assistance with this project. We would also like to thank Cody Flagg, Adam Kind, Austin Rutherford, Peter Chukran, Maddie Logowitz, Henry Grover, Jessica Mikenas, Mehmet Ozturk, and the other students and technicians that have helped with this project. Use of trade, product, or firm names is for information purposes only and does not constitute an endorsement by the U.S. Government. We also thank the handling editor and anonymous reviewers for helping considerably improve the manuscript.

References

Aubault, H, Webb, NP., Strong, CL., McTainsh, GH, Leys, JF, and Scanlan, JC. 2015. Grazing impacts on the susceptibility of rangelands to wind erosion: the effects of stocking rate, stocking strategy and land condition. Aeolian Research: v. 17, p. 89-99.

Ault, TR, Mankin, JS, Cook, BI, and Smerdon, JE. 2016. Relative impacts of mitigation, temperature, and precipitation on 21st-century megadrought risk in the American Southwest: Science Advances: v. 2, no. 10, p. e1600873.

Baddock, MC, Bullard, JE, and Bryant, RG. 2009. Dust source identification using MODIS: A comparison of techniques applied to the Lake Eyre Basin, Australia. Remote Sensing of Environment: v. 113, no. 7, p. 1511-1528.

Belnap, J, and Gillette, DA. 1997. Disturbance of biological soil crusts: Impacts on potential wind erodibility of sandy desert soils in southeastern Utah. Land Degradation & Development: v. 8, no. 4, p. 355-362.

Belnap, J, 1998. Vulnerability of desert biological soil crusts to wind erosion: the influences of crust development, soil texture, and disturbance. Journal of Arid Environments: v. 39, no. 2, p. 133-142.

Belnap, J, Phillips, SL, Herrick, JE, and Johansen, JR, 2007. Wind erodibility of soils at Fort Irwin, California (Mojave Desert), USA, before and after trampling disturbance: implications for land management. Earth Surface Processes and Landforms: v. 32, no. 1, p. 75-84.

Belnap, J, Reynolds, RL, Reheis, MC, Phillips, SL, Urban, FE, and Goldstein, HL. 2009. Sediment losses and gains across a gradient of livestock grazing and plant invasion in a cool, semi-arid grassland, Colorado Plateau, USA: Aeolian Research: v. 1, no. 1, p. 27-43.

Bestelmeyer, BT. 2006. Threshold Concepts and Their Use in Rangeland Management and Restoration: The Good, the Bad, and the Insidious: Restoration Ecology: v. 14, no. 3, p. 325-329.

Bestelmeyer, B. T., A. M. Ellison, W. R. Fraser, K. B. Gorman, S. J. Holbrook, C. M. Laney, M. D. Ohman, D. P. C. Peters, F. C. Pillsbury, A. Rassweiler, R. J. Schmitt, and S. Sharma. 2011. Analysis of abrupt transitions in ecological systems. Ecosphere 2:art129.

Bestelmeyer, BT, Tugel, AJ, Peacock Jr, GL, Robinett, DG, Shaver, PL, Brown, JR, Herrick, J E, Sanchez, H, and Havstad, KM, 2009, State-and-transition models for heterogeneous landscapes: a strategy for development and application: Rangeland Ecology & Management: v. 62, no. 1, p. 1-15.

Bullard, J, Baddock, M, McTainsh, G, and Leys, J. 2008. Sub-basin scale dust source geomorphology detected using MODIS. Geophysical Research Letters: v. 35, no. 15, p. n/a-n/a.

Chappell, A, McTainsh, G, Leys, J, and Strong, C. 2003. Using geostatistics to elucidate temporal change in the spatial variation of aeolian sediment transport Earth Surface Processes and Landforms: v. 28, no. 6, p. 567-585.

Chappell, A, and Webb, NP. 2016. Using albedo to reform wind erosion modelling, mapping and monitoring. Aeolian Research: v. 23, p. 63-78.

Conrad, O., and Wichmann, V., 2011, SAGA GIS (www.saga-gis.org): Hamburg, Germany.

Cook, AG, Weinstein, P, and Centeno, JA. 2005. Health effects of natural dust. Biological trace element research: v. 103, no. 1, p. 1.

Cook, BI, Ault, TR, and Smerdon, JE. 2015. Unprecedented 21st century drought risk in the American Southwest and Central Plains. Science Advances: v. 1, no. 1, p. e1400082.

Cook, BI, Miller, RL, and Seager, R. 2009. Amplification of the North American “Dust Bowl” drought through human-induced land degradation. Proceedings of the National Academy of Sciences: v. 106, no. 13, p. 4997-5001.

Copeland, SM, Bradford, JB, Duniway, MC, and Schuster, RM. 2017. Human impacts on the Colorado Plateau: potential impacts of overlapping land-use and climate in a sensitive dryland. Ecosphere: In Press.

Derbyshire, E. 2007. Natural minerogenic dust and human health. AMBIO: A Journal of the Human Environment: v. 36, no. 1, p. 73-77.

Draut, A. E., Hiza Redsteer, M., and Amoroso, L., 2013, Recent seasonal variations in arid landscape cover and aeolian sand mobility, Navajo Nation, southwestern United States: Climates, Landscapes, and Civilizations, p. 51-60.

Draut, A. E., Redsteer, M. H., and Amoroso, L., 2012, Vegetation, substrate, and eolian sediment transport at Teesto Wash, Navajo Nation, 2009-2012: US Geological Survey, 2328-0328.

Duniway, MC, Nauman, TW, Johanson, JK, Green, S, Miller, ME, Williamson, JC, and Bestelmeyer, BT. 2016. Generalizing Ecological Site Concepts of the Colorado Plateau for Landscape-Level Applications. Rangelands: v. 38, no. 6, p. 342-349.

Duniway, M. C., E. L. Geiger, T. J. Minnick, S. L. Phillips, and J. Belnap. *In Press*. Insights from long-term ungrazed and grazed watersheds in a salt desert Colorado Plateau ecosystem. *Rangeland Ecology & Management*.

Egan, T. 2006. The worst hard time: The untold story of those who survived the great American dust bowl. Houghton Mifflin Harcourt.

EPA-DRI-CSOSE. 2014. Method to Quantify Road Dust Particulate Matter Emissions (PM10 and/or PM2.5) from Vehicular Travel on Paved and Unpaved Roads

ELD Initiative. 2015. The value of land: Prosperous lands and positive rewards through sustainable land management. Available from www.eld-initiative.org.

ESRI. 2014. ArcGIS 10.3: Redlands, CA, Environmental Systems Research Institute.

Fick, S, Decker, C, Duniway, MC, and Miller, ME. 2016. Small-scale barriers mitigate desertification processes and enhance plant recruitment in a degraded semi-arid grassland. Ecosphere: v. 7, no. 6.

Field, JP, Belnap, J, Breshears, DD, Neff, JC, Okin, GS, Whicker, JJ, Painter, TH, Ravi, S, Reheis, MC, and Reynolds, RL. 2009. The ecology of dust. Frontiers in Ecology and the Environment: v. 8, no. 8, p. 423-430.

Flagg, CB, Neff, JC, Reynolds, RL, and Belnap, J. 2014. Spatial and temporal patterns of dust emissions (2004–2012) in semi-arid landscapes, southeastern Utah, USA. Aeolian Research: v. 15, p. 31-43.

Floyd, KW, & Gill, TE. 2011. The association of land cover with aeolian sediment production at Jornada Basin, New Mexico, USA. Aeolian Research: 3, 55-66

Fryrear, DW. 1986. A field dust sampler. Journal of Soil and Water Conservation. v. 41, no. 2, p. 117-120.

Fryrear, DW, Stout, JE, Hagen, LJ, and Vories, ED. 1991. Wind erosion: field measurement and analysis. Trans. ASAE: v. 34, no. 1, p. 155-160.

Gesch, DB. 2007. The National Elevation Dataset, *in* Maune, D., ed., Digital Elevation Model Technologies and Applications: The DEM Users Manual, American Society for Photogrammetry and Remote Sensing, p. 99-118.

Gesch, DB, Oimoen, M, Greenless, S, Nelson, C, Steuck, M, and Tyler, D. 2002. The National Elevation Dataset Photogrammetric Engineering and Remote Sensing: v. 68, no. 1, p. 5-11.

Gillette, D. A., 1977, Fine particulate emissions due to wind erosion: Transactions of the ASAE, v. 20, no. 5, p. 890-0897.

Gillette, DA. 1999. A qualitative geophysical explanation for hot spot dust emitting source regions. Contributions to Atmospheric Physics: v. 72, no. 1, p. 67-77.

Gillies, JA, Etyemezian, V, Kuhns, H, Nikolic, D, and Gillette, DA. 2005. Effect of vehicle characteristics on unpaved road dust emissions. Atmospheric Environment. v. 39, no. 13, p. 2341-2347.

Godfrey, AE, Everitt, BL, and Duque, JFM. 2008. Episodic sediment delivery and landscape connectivity in the Mancos Shale badlands and Fremont River system, Utah, USA. Geomorphology: v. 102, no. 2, p. 242-251.

Goossens, D., and Buck, B. J., 2012, Can BSNE (Big Spring Number Eight) samplers be used to measure PM10, respirable dust, PM2. 5 and PM1. 0?: Aeolian Research, v. 5, p. 43-49.

Goossens, D., and Offer, Z. Y., 2000, Wind tunnel and field calibration of six aeolian dust samplers: Atmospheric Environment, v. 34, no. 7, p. 1043-1057.

Gorelick, N, Hancher, M, Dixon, M, Ilyushchenko, S, Thau, D, & Moore, R. 2017. Google Earth Engine: Planetary-scale geospatial analysis for everyone. Remote Sensing of Environment.

Griffin, DW, Kellogg, CA, and Shinn, EA. 2001. Dust in the wind: long range transport of dust in the atmosphere and its implications for global public and ecosystem health. Global Change and Human Health: v. 2, no. 1, p. 20-33.

Hand, J. L., T. E. Gill, and B. A. Schichtel. 2017. Spatial and seasonal variability in fine mineral dust and coarse aerosol mass at remote sites across the United States. Journal of Geophysical Research: Atmospheres 122:3080-3097.

Hansen, Z. K., and Libecap, G. D., 2004, Small Farms, Externalities, and the Dust Bowl of the 1930's: National Bureau of Economic Research.

Hengl, T., de Jesus, J. M., Heuvelink, G. B. M., Gonzalez, M. R., Kilibarda, M., Blagotić, A., Shangguan, W., Wright, M. N., Geng, X., and Bauer-Marschallinger, B., 2017, SoilGrids250m: Global gridded soil information based on machine learning: PloS one, v. 12, no. 2, p. e0169748.

Hijmans, RJ, van Etten, J, Cheng, J, Mattiuzzi, M, Sumner, M, Greenberg, JA, Lamigueiro, OP, Bevan, A, Racine, EB, and Shortridge, A. 2016. Package 'raster': R package. https://cran. r-project. org/web/packages/raster/index. html (accessed 1 October 2016).

Li, J, Okin, GS, Skiles, SM, and Painter, TH. 2013. Relating variation of dust on snow to bare soil dynamics in the western United States. Environmental Research Letters: v. 8, no. 4, p. 044054.

Lee, J.A., Baddock, M.C., Mbuh, M.J., & Gill, T.E. (2012). Geomorphic and land cover characteristics of aeolian dust sources in West Texas and eastern New Mexico, USA, Aeolian Research, 3, 459-466.

Lee, J.A., & Gill, T.E. (2015). Multiple causes of wind erosion in the Dust Bowl, Aeolian Research, 19, 15-36.

Lowry, J, Ramsey, RD, Thomas, K, Schrupp, D, Sajwaj, T, Kirby, J, Waller, E, Schrader, S, Falzarano, S, Langs, L, Manis, G, Wallace, C, Schulz, K, Comer, P, Pohs, K, Rieth, W, Velasquez, C, Wolk, B, Kepner, W, Boykin, K, O'Brien, L, Bradford, D, Thompson, B, and Prior-Magee, J. 2007. Mapping moderate-scale land-cover over very large geographic areas within a collaborative framework: A case study of the Southwest Regional Gap Analysis Project (SWREGAP). Remote Sensing of Environment: v. 108, no. 1, p. 59-73.

Lu, H, and Shao, Y. 1999. A new model for dust emission by saltation. Journal of Geophysical Research: v. 104, p. 16827-16842.

Lu, H. and Shao, Y., 2001. Toward quantitative prediction of dust storms: an integrated wind erosion modelling system and its applications. Environmental Modelling & Software: v. 16, no. 3, p. 233-249.

Maindonald, JH, Braun, WJ, and Braun, MWJ. 2015. Package 'DAAG' (Data Analysis and Graphics Data and Functions: https://cran.r-project.org/web/packages/DAAG/DAAG.pdf).

Marsett, RC, Qi, J, Heilman, P, Biedenbender, SH, Watson, MC, Amer, S, Weltz, M, Goodrich, D, and Marsett, R. 2006. Remote sensing for grassland management in the arid southwest. Rangeland Ecology & Management: v. 59, no. 5, p. 530-540.

McBratney, AB, Santos, MLM, and Minasny, B. 2003. On digital soil mapping. Geoderma: v. 117, no. 1-2, p. 3-52.

Miller, ME, Belote, RT, Bowker, MA, and Garman, SL. 2011. Alternative states of a semiarid grassland ecosystem: implications for ecosystem services. Ecosphere: v. 2, no. 5, p. 1-18.

Miller, ME, Bowker, MA, Reynolds, RL, and Goldstein, HL. 2012. Post-fire land treatments and wind erosion–lessons from the Milford Flat Fire, UT, USA. Aeolian Research: v. 7, p. 29-44.

Montgomery, D. R., 2007, Soil erosion and agricultural sustainability: Proceedings of the National Academy of Sciences, v. 104, no. 33, p. 13268-13272.

Morrison, SJ, Goodknight, CS, Tigar, AD, Bush, RP, and Gil, A. 2012. Naturally occurring contamination in the Mancos Shale. Environmental science & technology: v. 46, no. 3, p. 1379-1387.

Munson, SM, Belnap, J, and Okin, GS. 2011. Responses of wind erosion to climate-induced vegetation changes on the Colorado Plateau. Proceedings of the National Academy of Sciences: v. 108, no. 10, p. 3854-3859.

Nauman, T. 2017. Rangeland condition and cattle use assessment observations, May 3, 2017.

Nauman, TW, and Duniway, MC. 2016. The Automated Reference Toolset: A Soil-Geomorphic Ecological Potential Matching Algorithm. Soil Science Society of America Journal: v. 80, no. 5, p. 1317-1328.

Nauman, TW, Duniway, MC, Villarreal, ML, and Poitras, TB. 2017. Disturbance automated reference toolset (DART): Assessing patterns in ecological recovery from energy development on the Colorado Plateau. Science of The Total Environment.

Neff, JC, Ballantyne, AP, Farmer, GL, Mahowald, NM, Conroy, JL, Landry, CC, Overpeck, JT, Painter, TH, Lawrence, CR, and Reynolds, RL. 2008. Increasing eolian dust deposition in the western United States linked to human activity. Nature Geoscience: v. 1, no. 3, p. 189-195.

NREL. 2015. Wind Data - 50m height (http://www.nrel.gov/gis/data_wind.html).

Okin, GS. 2005. Dependence of wind erosion and dust emission on surface heterogeneity: Stochastic modeling. Journal of Geophysical Research: Atmospheres: v. 110, no. D11.

Okin, G. S., Bullard, J. E., Reynolds, R. L., Ballantine, J.-A. C., Schepanski, K., Todd, M. C., Belnap, J., Baddock, M. C., Gill, T. E., and Miller, M. E., 2011, Dust: Small-scale processes with global consequences: Eos, v. 92, no. 29.

Okin, GS, Gillette, DA, and Herrick, JE. 2006, Multi-scale controls on and consequences of aeolian processes in landscape change in arid and semi-arid environments. Journal of Arid Environments: v. 65, no. 2, p. 253-275.

Okin, G. S., Murray, B., and Schlesinger, W. H., 2001a, Degradation of sandy arid shrubland environments: observations, process modelling, and management implications: Journal of Arid Environments, v. 47, no. 2, p. 123-144.

Okin, G. S., Murray, B., and Schlesinger, W. H., 2001b, Desertification in an arid shrubland in the southwestern United States, Land Degradation, Springer, p. 53-70.

Omernik, J, and Griffith, G. 2014. Ecoregions of the Conterminous United States: Evolution of a Hierarchical Spatial Framework. Environmental Management: v. 54, no. 6, p. 1249-1266.

Padgett, PE, Meadows, D, Eubanks, E, and Ryan, WE. 2008. Monitoring fugitive dust emissions from off-highway vehicles traveling on unpaved roads and trails using passive samplers. Environmental monitoring and assessment: v. 144, no. 1-3, p. 93-103.

Painter, TH, Deems, JS, Belnap, J, Hamlet, AF, Landry, CC, and Udall, B. 2010. Response of Colorado River runoff to dust radiative forcing in snow. Proceedings of the National Academy of Sciences: v. 107, no. 40, p. 17125-17130.

Painter, T.H., Skiles, S.M., Deems, J.S., Brandt, W.T., Dozier, J., 2018, Variation in rising limb of Colorado River snowmelt runoff hydrograph controlled dust radiative forcing in snow. Geophysical Research Letters, 44, https://doi.org/10.1002/2017GL075826

Parajuli, SP, ZL Yang, and G. Kocurek. 2014. Mapping erodibility in dust source regions based on geomorphology, meteorology, and remote sensing. Journal of Geophysical Research: Earth Surface: 119:1977-1994.

Peters, D. P. C., O. E. Sala, C. D. Allen, A. Covich, and M. Brunson. 2007. Cascading events in linked ecological and socioeconomic systems. Frontiers in Ecology and the Environment 5:221-224.

Pliler, R, and Adams, JAS. 1962. The distribution of thorium, uranium, and potassium in the Mancos Shale. Geochimica et Cosmochimica Acta: v. 26, no. 11, p. 1115-1135.

Poitras, T. B., Villarreal, M. L., Waller, E. K., Nauman, T. W., Miller, M. E., and Duniway, M. C., 2018, Identifying optimal remotely-sensed variables for ecosystem monitoring in Colorado Plateau drylands: Journal of Arid Environments.

Prism Climate Group. 2010. 30-yr Normals (1981-2010) (http://www.prism.oregonstate.edu/normals/).

R Core Development Team. 2005. R: A language and environment for statistical computing: R foundation for Statistical Computing.

Reheis, M. C., and Kihl, R., 1995, Dust deposition in southern Nevada and California, 1984–1989: Relations to climate, source area, and source lithology: Journal of Geophysical Research: Atmospheres, v. 100, no. D5, p. 8893-8918.

Ripley, B, Venables, B, Bates, DM, Hornik, K, Gebhardt, A, Firth, D, and Ripley, MB. 2013. Package 'MASS' : Cran R, https://cran.r-project.org/web/packages/MASS/index.html.

Sankey, J.B., Germino, M.J., Benner, S.G., Glenn, N.F. and Hoover, A.N., 2012. Transport of biologically important nutrients by wind in an eroding cold desert. Aeolian Research, (7), pp.17-27.

Sankey, J.B., Germino, M.J. and Glenn, N.F., 2012. Dust supply varies with sagebrush microsites and time since burning in experimental erosion events. Journal of Geophysical Research: Biogeosciences, 117(G1).

Sayre, N. F. 2017. The politics of scale: A history of rangeland science. University of Chicago Press.

Schlaepfer, D. R., Bradford, J. B., Lauenroth, W. K., Munson, S. M., Tietjen, B., Hall, S. A., Wilson, S. D., Duniway, M. C., Jia, G., Pyke, D. A., Lkhagva, A., and Jamiyansharav, K., 2017, Climate change reduces extent of temperate drylands and intensifies drought in deep soils: Nature Communications, v. 8, p. 14196.

Schmidt, J, and Hewitt, A. 2004. Fuzzy land element classification from DTMs based on geometry and terrain position. Geoderma: v. 121, no. 3-4, p. 243-256.

Shao, Y. 2008. Physics and modelling of wind erosion. Springer Science & Business Media.

Shao, Y, and Leslie, LM. 1997. Wind erosion prediction over the Australian continent. Journal of Geophysical Research: Atmospheres: v. 102, no. D25, p. 30091-30105.

Shao, Y., McTainsh, G. H., Leys, J. F., and Raupach, M. R. 1993. Efficiencies of sediment samplers for wind erosion measurement: Soil Research, v. 31, no. 4, p. 519-532.

Statwick, J, and Sher, AA. 2017. Selenium in soils of western Colorado. Journal of Arid Environments: v. 137, p. 1-6.

Sterk, G, and Stein, A. 1997. Mapping wind-blown mass transport by modeling variability in space and time. Soil Science Society of America Journal: v. 61, no. 1, p. 232-239.

Stokes, WML, and Mobley, CM. 1954. Geology and Uranium Deposits of the Thompson Area, Grand County, Utah.

Tarboton, DG. 1997. A new method for the determination of flow directions and upslope areas in grid digital elevation models. Water Resources Research. v. 33, no. 2, p. 309-319.

Thomas, K. A., and Redsteer, M. H., 2016. Vegetation of semi-stable rangeland dunes of the Navajo Nation, Southwestern USA: Arid Land Research and Management, v. 30, no. 4, p. 400-411.

Trenberth, K. E., Dai, A., Van Der Schrier, G., Jones, P. D., Barichivich, J., Briffa, K. R., and Sheffield, J., 2014, Global warming and changes in drought: Nature Climate Change, v. 4, no. 1, p. 17.

UAGRC. 2015. Utah Roads and Highway System (http://gis.utah.gov/data/sgid-transportation/roads-system/).

UNEP, WMO, UNCCD. 2016. Global Assessment of Sand and Dust Storms. United Nations Environment Programme, Nairobi. https://public.wmo.int/en/resources/library/global-assessment-of-sand-and-dust-storms

United States Department of Agriculture, NRCS. 2010a. Soil Survey of Arches National Park, Utah. Accessible online at: http://soils.usda.gov/survey/printed_surveys/.

United States Department of Agriculture, NRCS. 2010b. Soil Survey of Canyonlands National Park, Utah. Accessible online at: http://soils.usda.gov/survey/printed_surveys/.

USDOI-BLM-CCDO. 2013. Analysis of the Management Situation for the Canyon Country District Office Moab Master Leasing Plan and Associated Environmental Impact Statement.

Villarreal, M. L., Norman, L. M., Buckley, S., Wallace, C. S. A., and Coe, M. A., 2016, Multi-index time series monitoring of drought and fire effects on desert grasslands: Remote Sensing of Environment, v. 183, p. 186-197.

Wagner, LE. 2013. A history of wind erosion prediction models in the United States Department of Agriculture: The Wind Erosion Prediction System (WEPS). Aeolian Research: v. 10, p. 9-24.

Webb, NP, Herrick, JE, and Duniway, MC. 2014. Ecological site-based assessments of wind and water erosion: informing accelerated soil erosion management in rangelands. Ecological Applications: v. 24, no. 6, p. 1405-1420.

Webb, N.P., Pierre, C., 2018. Quantifying anthropogenic dust emissions. Earth's Future. doi:10.1002/2017EF000766

Webb, N. P., Herrick, J. E., Van Zee, J. W., Courtright, E. M., Hugenholtz, C. H., Zobeck, T. M., Okin, G. S., Barchyn, T. E., Billings, B. J., Boyd, R., Clingan, S. D., Cooper, B. F., Duniway, M. C., Derner, J. D., Fox, F. A., Havstad, K. M., Heilman, P., LaPlante, V., Ludwig, N. A., Metz, L. J., Nearing, M. A., Norfleet, M. L., Pierson, F. B., Sanderson, M. A., Sharratt, B. S., Steiner, J. L., Tatarko, J., Tedela, N. H., Toledo, D., Unnasch, R. S., Van Pelt, R. S., and Wagner, L., 2016, The National Wind Erosion Research

Network: Building a standardized long-term data resource for aeolian research, modeling and land management: Aeolian Research, v. 22, p. 23-36.

Webb, NP, Zee, JWV, Karl, JW, Herrick, JE, Courtright, EM, Billings, BJ, Boyd, R, Chappell, A, Duniway, MC, Derner, JD, Hand, JL, Kachergis, E, McCord, SE, Newingham, BA, Pierson, FB, Steiner, JL, Tatarko, J, Tedela, NH, Toledo, D, and Pelt, RSV. 2017. Enhancing Wind Erosion Monitoring and Assessment for U.S. Rangelands. Rangelands.

von Holdt, J. R., Eckardt, F. D., and Wiggs, G. F. S., 2017, Landsat identifies aeolian dust emission dynamics at the landform scale: Remote Sensing of Environment, v. 198, no. Supplement C, p. 229-243.

Yao, J., D. P. C. Peters, K. M. Havstad, R. P. Gibbens, and J. E. Herrick. 2006. Multi-Scale Factors and Long-Term Responses of Chihuahuan Desert Grasses to Drought. Landscape Ecology 21:1217-1231.

Tables

Table 1. Summary of road types used for creating road buffers used for creating road dust modeling raster mask.

Road type (CARTOCODE)	obs 1	obs 2	obs 3	obs 4	obs 5	width (m)	Excluded surface types (SURFTYPE)
Other Fed Aid Eligible Local Rds	9.00	8.00	10.00	15.00	7.00	9.00	Paved, 100
Other Local, Neighborhood, Rural Roads	3.00	3.00	5.00	3.50	2.00	3.00	Paved, 100
Other	3.00	7.00	2.00	3.00	5.50	3.00	Paved, 100
Non-road feature	8.00	3.00	2.50	3.00	4.00	3.00	Paved, 100
Major Local Roads, Unpaved	7.50	5.00	10.00	13.00	6.00	7.50	Paved, 100

Table 2. Annual climate regression model coefficients

Heavily Grazed Blowout Regression

Variable†	Est.	Std. Err.	t	Pr(>|t|)
precip. (mm)	0.47	0.193	2.43	0.045
mean wind speed (m/s)	-33.11	12.85	-2.58	0.037
Precip / wind speed	-1.312	0.527	-2.49	0.042

Adjusted R^2 = 0.62, F-statistic = 6.26, p = 0.021, DF of 3 & 7

One-out Cross Validation: R^2 = 0.44, RMSE = 1.65 g m^{-2} d^{-1}

† Flux was natural logarithm transformed for normality

Heavily Grazed Intact Regression

Variable	Est.	Std. Err.	t	Pr(>|t|)
temp. (C)	8.33	2.31	3.61	0.007
precip. (mm)	-0.47	0.161	-2.92	0.019
Precip / temp	5.095	1.9	2.68	0.028

Adjusted R^2 = 0.66, F-statistic = 8.0, p = 0.01, DF of 3 & 8

One-out Cross Validation: R^2 = -0.39*, RMSE = 4.77 g m^{-2} d^{-1}

*Outlier in 2009, R^2 = 0.58, RMSE = 2.71 without

Light/Not Grazed Regression

Variable	Est.	Std. Err.	t	Pr(>|t|)
temp. (C)	10.07	3.86	2.61	0.048
mean wind speed (m/s)	38.43	16.69	2.3	0.069
Temp * windspeed	-3.61	1.44	-2.51	0.054

Adjusted R^2 = 0.67, F-statistic = 6.44, p = 0.036, DF of 3 & 5

One-out Cross Validation: R^2 = 0.33, RMSE = 0.54 g m^{-2} d^{-1}

Off Road Vehicle Regression

Variable	Est.	Std. Err.	t	Pr(>|t|)
% time >4.4 m/s wind	8472	1868	4.54	0.14
precip. (mm)	-2.396	0.61	-4.0	0.16
temp. (C)	-41.71	21.7	-1.92	0.31

Adjusted R^2 = 0.92, F-statistic = 16.2, p = 0.18, DF of 3 & 1

One-out Cross Validation: R^2 = -0.431, RMSE = 176 g m^{-2} d^{-1}

Off Road Vehicle Control Regression

Variable††	Est.	Std. Err.	t	Pr(>|t|)
precip. (mm)	0.15	0.036	4.2	0.052
% time > 4.4 m/s wind	120.8	25.93	4.66	0.043
precip*% time >4.4 m/s	-0.692	0.158	-4.4	0.048

Adjusted R^2 = 0.95, F-statistic = 33, p = 0.03, DF of 3 & 2

One-out Cross Validation: R^2 = 0.63, RMSE = 1.61 g m^{-2} d^{-1}

†† Flux was base-10 logarithm transformed for normality

Table 3. Predictive multiple regression model performance and parameters ordered by p-value for rangeland sites. Coefficients are for association with log_{10}(flux). RMSE values are back transformed from log_{10} scale to flux units.

Variable	Estimate	Std. Error	t	Pr(>|t|)	Variable Description
redbluend	7.56	1.970	3.83	0.00038	Landsat red to blue band normalized difference ratio
swregap118	0.73	0.200	3.65	0.00066	Southwest ReGAP: Invasive Southwest Riparian Woodland and Shrubland dummy variable
relmnht8	0.15	0.041	3.57	0.00084	Local elevation relative to the mean elevation within 8 pixel radius.
redgreennd	-10.30	3.020	-3.40	0.00138	Landsat red to green band normalized difference ratio
slplp3	0.24	0.072	3.29	0.00191	Slope gradient after low pass (3x3) filter
redswir1nd	-5.28	1.760	-3.00	0.00437	Landsat red to SWIR1 band normalized difference ratio
satvi14	-8.8E-04	3.1E-04	-2.88	0.00599	SATVI vegetation index median from 05/2014-09/2014
twilp3	0.08	0.028	2.83	0.00676	Topographic wetness index after low pass filter
relht1	-0.72	0.255	-2.83	0.00677	Relative height (above local minimum) within one pixel radius
swness	-0.17	0.065	-2.54	0.01455	Aspect index (1 to -1) of southwest to northeast: cos(aspect - 225)
LFelems100	0.45	0.197	2.27	0.02805	Landform: Plains dummy variable (Schmidt and Hewitt, 2004).
relmnht16	-0.02	0.011	-2.27	0.02809	Local elevation relative to the mean elevation within 16 pixel radius.
swir1swir2nd	-4.84	2.600	-1.86	0.06883	Landsat SWIR1 to SWIR2 band normalized difference ratio
pptann	2.9E-03	0.002	1.80	0.0788	Annual precipitation normal for 1981-2010, resampled to 30m by cubic convolution (PRISM Climate Group, 2010)
elevm	-6.0E-04	4.0E-04	-1.51	0.13718	Elevation in meters from National Elevation Dataset.
tmnann	0.15	0.112	1.36	0.17879	Annual temperature normal for 1981-2010, resampled to 30m by cubic convolution (PRISM Climate Group, 2010)
swregap40	-0.17	0.126	-1.35	0.18408	Southwest ReGAP: Inter-Mountain Basins Mat Saltbush Shrubland dummy variable.
MRRTF	0.04	0.034	1.29	0.20279	Multiple resolution ridgetop flatness index (Conrad and Wichmann, 2011)

Adjusted R^2 = 0.57, F-statistic = 5.76, p = 6.4×10^{-07}, DF of 18 and 47

11-Fold Cross Validation: R^2 = 0.39, RMSE = 1.98 g m^{-2} day^{-1}

Table 4. Predictive multiple regression model performance and parameters ordered by p-value for road sites. Coefficients are for association with log_{10}(flux) before transformation. RMSE values are back transformed from log_{10} scale.

Variable	estimate	std error	t-value	Pr(>|t|)	Variable Description
redgreennd	6.28	1.73	3.63	0.0015	Landsat red to green band normlized difference ratio: median 5/2014-9-2014
swregap36	-1.4E+00	0.394	-3.63	0.0015	Southwest ReGap CO Plateau Pinon-Juniper Woodland binary
elevm	2.9E-03	0.000867	3.37	0.0028	Elevation in meters - National Elevation Dataset
swregap48	-1.1E+00	0.361	-3.04	0.0059	Southwest ReGap Inter-Mtn Basins Big Sagebrush Shrubland binary
pptsmrt	-1.3E+01	5.1	-2.47	0.0219	Ratio of summer June-Sept. to total annual precipitation from normal for 1981-2010, resampled to 30m by cubic convolution (PRISM Climate Group, 2010)
swregap108	-5.4E-01	0.25	-2.14	0.0441	Southwest ReGap Southern Colorado Plateau Sand Shrubland
swregap53	-4.1E-01	0.2	-2.05	0.0525	Southwest ReGap CO Plateau Blackbrush-Mormon-tea Shrubland
sness	1.3E-01	0.067	1.91	0.0691	Aspect index (1 to -1) of south to north: cos(aspect - 180)
pscsmod10	-0.18	0.0955	-1.88	0.0733	Fine-loamy soil particle size class binary variable (Nauman & Duniway, 2016)
pscsmod15	-0.22	0.132	-1.65	0.1130	Loamy soil particle size class binary variable (Nauman & Duniway, 2016)

Adjusted $R^2 = 0.516$, F-statistic = 4.41, p = 0.0018, DF of 10 and 22

5-Fold Cross Validation: $R^2 = 0.30$, RMSE = 1.69 g m^{-2} day^{-1}

Table 5. Relative dust emission source estimates based spatial models of sediment *q* for both unpaved roads and rangelands in study area. Three scenarios for inference constraints (0, 5, and 10% of minimum of maximum intervals) are shown along with the amount of total road and rangeland areas represented by each. Estimates are based on model predictions, and unpaved road *q* values are corrected for regional southwest wind proportionality.

Land Use Type	Inference Scenario	Model Area (km)	% of Total Area*	Mean *q* (g m^{-2} day^{-1})	Summed Regional Flux	% of *q* Regionally
road	0%	59	73.9%	38.69	4.84E+13	8.2%
range	0%	5302	52.2%	4.79	5.42E+14	91.8%
road	5%	67	84.7%	38.53	5.52E+13	7.4%
range	5%	6236	61.5%	5.19	6.90E+14	92.6%
road	10%	71	89.1%	39.28	5.92E+13	6.9%
range	10%	6725	66.3%	5.61	8.04E+14	93.1%

* Total area of 1) all unpaved roads, or 2) Undeveloped rangelands within the study area.

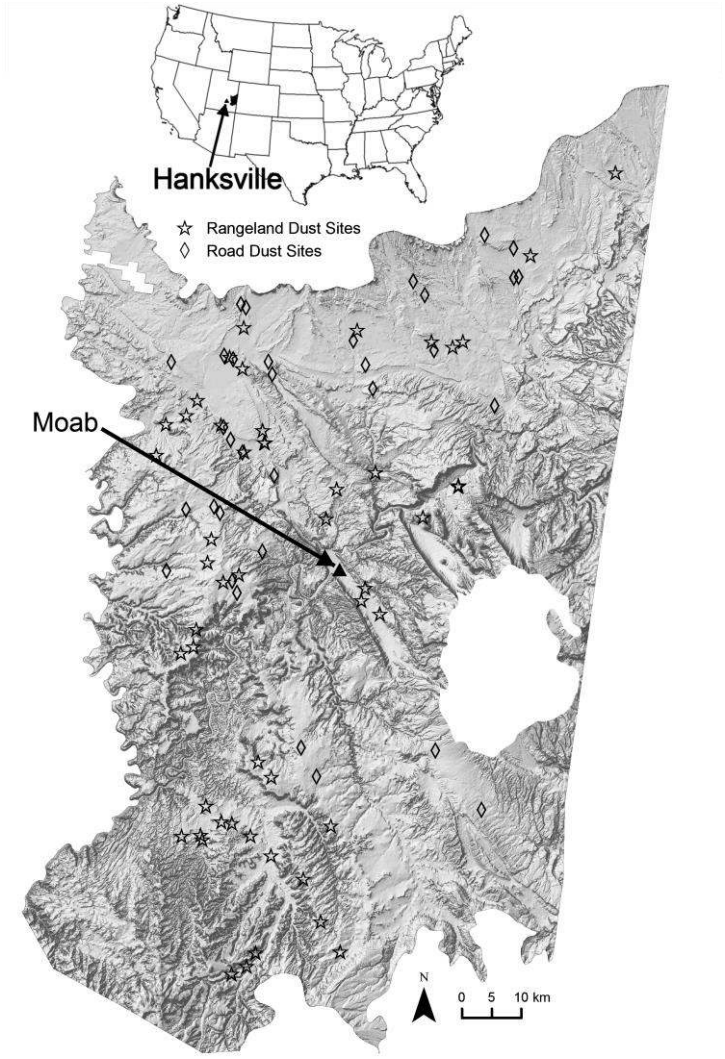

Figure. 1. Study area for regional dust source spatial predictions with dust monitoring sites symbolized by road or rangeland networks. Area outlined was mainly defined by EPA Level 4 ecoregions (Omernik and Griffith, 2014) while excluding the higher elevation areas in the La Sal Mountains (hole in east side of map). Some rangeland sites were not in the spatial prediction area, but were nearby in similar soil, vegetation and climatic areas as represented in modeling area. The off-highway vehicle (OHV) area monitored was near Hanksville, Utah, about 125km west of the spatial prediction area, and also has similar soils and climate.

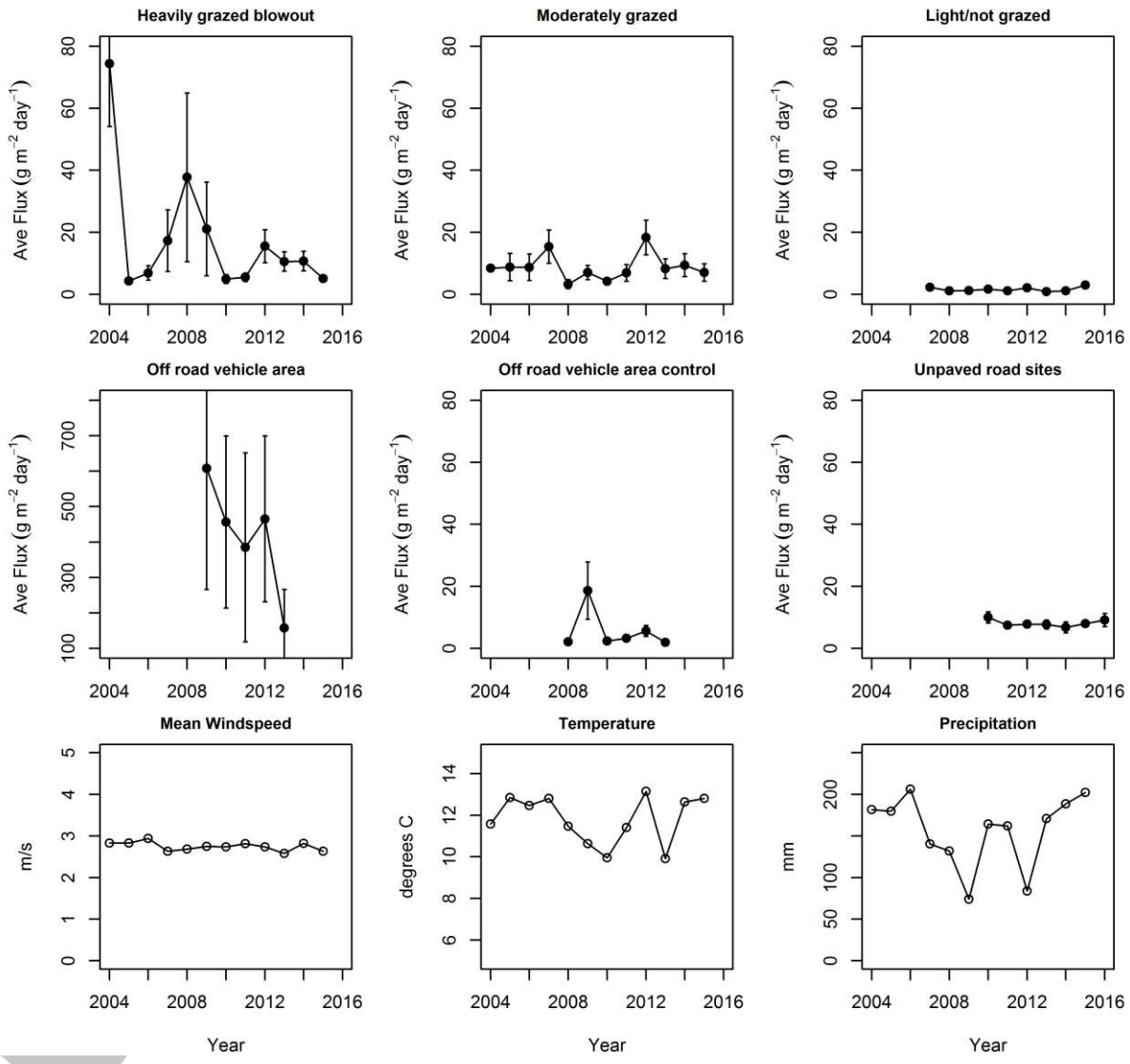

Figure 2. Annual trends in dust monitoring sites with standard error bars. The "Light/not grazed" error bars are too small to see due to minimal variation among those sites. Note the differing y-axis range at OHV sites where the highest fluxes of all sites were observed. Road flux values are not corrected for southwest wind proportionality. Annual averages of wind speed (m/s), temperature (C), and precipitation (mm) at the Canyonlands Airport (KCNY) are also graphed during same time period.

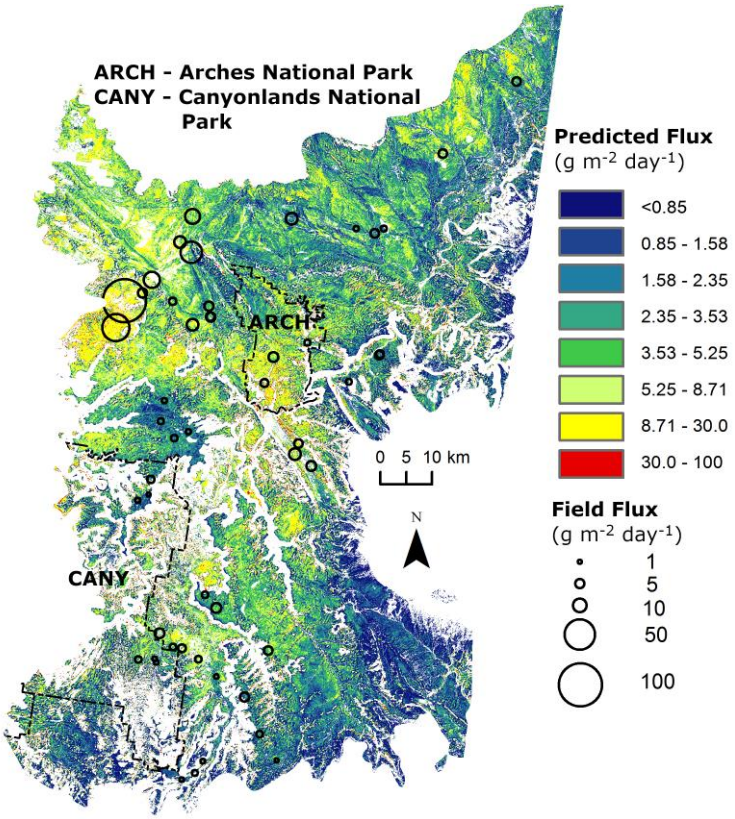

Figure 3. Prediction map showing rangeland sediment horizontal mass flux (*q*) at 100 cm height above ground level. Predictions are shown across the area within the 10% inference mask. Actual *q* measurements used in model preparation are overlaid as proportionally sized circles.

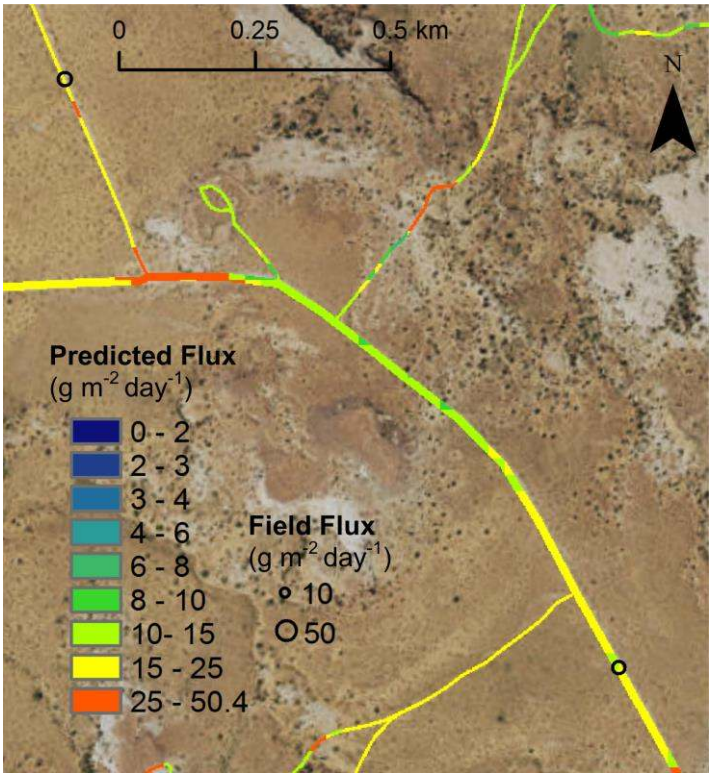

Figure 4. Area near Canyonlands National Park showing unpaved road sediment horizontal mass flux (*q*) predictions overlaid with the field BSNE collection sites represented as circles sized proportionally to flux. Variation in sediment *q* predictions tended to follow surface colors.

Figure 5. Heavily grazed blowout area east of Green River, Utah where high *q* values have been recorded consistently since 2009. BSNE tower is downwind near the line of shrubs in middle of photo. In this area active dunes are encroaching on shale derived alluvial areas creating a potential for sand saltation initiating dust emission from finer textured shale soils. In encroachment zone perennial vegetation is dying and several exotics (e.g., *Salsola sp.*) have invaded.

Appendix A. Raster variables used for spatial dust predictions.

Source	Variable	Description
National Elevation Dataset ~30-meter resolution 'TOPO' variables	NWNESS	index from 1 to -1 of how northwest (1) or southeast (-1) a site faces: Cosine(aspect – 315)
	WESTNESS	index from 1 to -1 of how west (1) or east (-1) a site faces: Cosine(aspect – 270)
	SOUTHNESS	index from 1 to -1 of how south (1) or north (-1) a site faces: Cosine(aspect – 180)
	SWNESS	index from 1 to -1 of how southwest (1) or northeast (-1) a site faces: Cosine(aspect – 225)
	ELEVm	elevation in meters
	TCURVLP3	curvature perpendicular to the slope direction (Conrad and Wichmann, 2011)
	PCURVLP3	curvature parallel to the slope direction (Conrad and Wichmann, 2011)
	PROTINDEX	Protection Index of surrounding topography (Conrad and Wichmann, 2011)
	SLPLP3	slope gradient in degrees
	MRRTF	multiple resolution ridgetop flatness index (Conrad and Wichmann, 2011)
	MRVBF	multiple resolution valley bottom flatness index (Conrad and Wichmann, 2011)
	TWILP3	topographic wetness index, also called compound topographic index
	CALP3	upstream contributing area (Using Dinf, Conrad and Wichmann, 2011; Tarboton, 1997)
	RELHT (1,2,n..128)	Height of cell above the local minimum elevation in n-pixel radius n =1,2,4,8,16,32,64,128 (By comparing to Focal Statistics minimum tool, ESRI, 2014)
	RELMNHT (1,2,n..128)	Height of cell above the local mean elevation in n-pixel radius n =1,2,4,8,16,32,64,128 (By comparing to Focal Statistics mean tool, ESRI, 2014)
	LFELEMS	Landform classification system using DEM: landform elements (Conrad and Wichmann, 2011; Schmidt and Hewitt, 2004)
SWREGAP	swregap_nm	SW vegetation and landcover map (Lowry et al., 2007)
NREL Wind	wind	Wind potential at 50m height from NREL: (NREL, 2015).
PRISM	temp_ann ppt_ann ppt_ratio ppt13 ppt13_0709 ppt14 ppt14_0709	MAT, MAP, seasonal precipitation: ratio of June-Sep/annual, 2013 precipitation, July-September 2013 precipitation, 2014 precipitation, and July-September 2014 precipitation. PRISM 1981-2010, 800m (PRISM Climate Group, 2010): cubic resample to 30 meter resolution.
Landsat 8 ratios	redbluend redgreennd redswir1nd swir1nirnd swir1swir2nd satvi13 satvi14	red/blue, red/green, red/swir1, swir1/swir2, swir1/nir as normalized difference indices. 'LS' geology ratios included the red/blue, red/green and swir1/swir2 as well as median soil adjusted total vegetation index for May thru September for 2013 and 2014 following Nauman et al., (2017).
Soil particle size classes	pscsmod	USDA particle size class in the control section modified by Nauman and Duniway (2016)

Appendix B. Google Earth Engine Code for SATVI creation.

```
var Lfact = .9;
var jsonstring=null;
var cloudshadow = ee.Geometry.Point([-108.7564, 36.1445]);
var hazyarea = ee.Geometry.Point([-109.482879,39.3791604]);

function calc_satvi(image_in, swir1_in, swir2_in){
  return image_in.expression('((1.9 * (swir1 - red)) / (swir1 + red + .9)) - swir2/2',
    {'swir1' : swir1_in, 'swir2': swir2_in, 'red': image_in.select('B4')});
}

function export_image(image_in, task_name_in) {
Export.image(image_in, task_name_in,
 {driveFileNamePrefix: 'UT'+task_name_in, scale: 30, maxPixels: 1400000000, region: jsonstring});
}
function Mosaic() {
// Define boundary of clip extent
var polygon = ee.FeatureCollection('ft:1xFxk4nOLf5q4D04ibV9SUdPvf1jLVp2HTKz4rqDX');
// Cloud Index Value
// 61440 = Cloudy (high probability) Cirrus
// 53248 = Cloudy (high probability) Non-Cirrus
// 28672 = Cloudy (low probability) Cirrus
var collectionnames=['LANDSAT/LC8_SR','LC8_L1T_TOA'];
// Change later to scenes from May thru September 2013
var startDate = new Date('5/15/2013');
var endDate = new Date('9/30/2013');
var collection = ee.ImageCollection(collectionnames[1])
   .filterDate(startDate, endDate);
var srcollection = ee.ImageCollection(collectionnames[0])
    .filterDate(startDate, endDate);
```

```
// From Noel at Google
var maskL8 = function(image) {
  var quality = image.select( 'BQA' );
  var cloud01 = quality.eq(61440);
  var cloud02 = quality.eq(53248);
  var cloud03 = quality.eq(28672);
  var maskedImage = image.mask().and(cloud01.or(cloud02).or(cloud03).not());
  return image.mask(maskedImage);
};

var VizParams = {min:0, max:0.7, 'bands':'B4,B3,B2'};
centerMap(-109.65,38.64);

// Select median pixels and clip
var image2 = collection.median().clip(polygon);
Map.addLayer(polygon,  {color: 'FFFF00'}, 'study area');
Map.setCenter(-111,38,7);
var collectionMasked = collection.map(maskL8);
var image3 = collectionMasked.median().clip(polygon);
addToMap(image3, VizParams, "With Cloud Mask",true);
var swir2 = image3.select('B7');
var swir1 = image3.select('B6');
var satvi = calc_satvi(image3, swir1, swir2);
var satvi_10k = satvi.multiply(10000)
var satvi_int = satvi_10k.round();
Map.addLayer(satvi_int, {min:-10000, max:10000}, 'satvi_int');
export_image(satvi_int, 'l8satvi_int');

} //end of function
Mosaic();
```